AD-A169 948 FINITE ELEMENT AND EXPERIMENTAL STUDIES OF CREEP CRACK 1/1
INITIATION OF RENE.. (U) MASSACHUSETTS INST OF TECH
CAMBRIDGE DEPT OF AERONAUTICS AND A.. T H PIAN ET AL.
UNCLASSIFIED 20 FEB 85 AFOSR-TR-86-0400 AFOSR-82-0320 F/G 11/6 NL

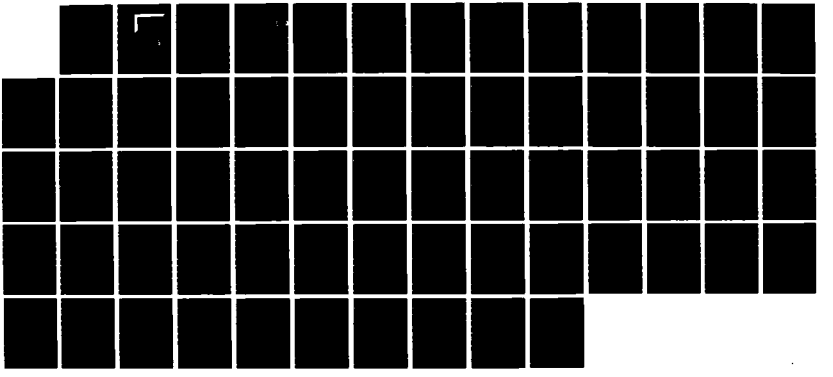

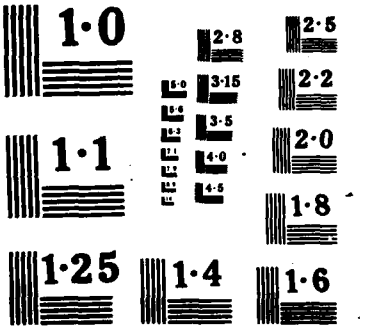
1·0
1·1
1·25
1·4
1·6
1·8
2·0
2·2
2·5
2·8
3·15
3·5
4·0
4·5

FINITE ELEMENT AND EXPERIMENTAL STUDIES OF CREEP CRACK INITIATION OF RENE-95 SUPERALLO

by

Theodore H.H. Pian
Pedro J. Sifre
Michael J. Lee

DEPARTMENT OF
AERONAUTICS AND ASTRONAUTICS
MASSACHUSETTS INSTITUTE OF TECHNOLOGY
CAMBRIDGE, MASSACHUSETTS 02139

FINITE ELEMENT AND EXPERIMENTAL STUDIES OF CREEP CRACK INITIATION OF RENE-95 SUPERALLOY

by

Theodore H.H. Pian
Pedro J. Sifre
Michael J. Lee

Final Report of Research Grant No.: AFOSR-82-0320

Submitted To:

U.S. Air Force
Office of Scientific Research
Bolling Air Force Base, D.C. 20332

Gas Turbine and Plasma Dynamics Laboratory
Department of Aeronautics and Astronautics
Massachusetts Institute of Technology
Cambridge, Massachusetts 02139

February, 1985

SECURITY CLASSIFICATION OF THIS PAGE

REPORT DOCUMENTATION PAGE

1a. REPORT SECURITY CLASSIFICATION: UNCLASSIFIED	1b. RESTRICTIVE MARKINGS
2a. SECURITY CLASSIFICATION AUTHORITY	3. DISTRIBUTION/AVAILABILITY OF REPORT: UNCLASSIFIED UNLIMITED
2b. DECLASSIFICATION/DOWNGRADING SCHEDULE	
4. PERFORMING ORGANIZATION REPORT NUMBER(S)	5. MONITORING ORGANIZATION REPORT NUMBER(S): AFOSR-TR- 86-0488
6a. NAME OF PERFORMING ORGANIZATION: Dept of Aeronautics & Astronautics, Massachusetts Inst. of Tech.. (6b. OFFICE SYMBOL (If applicable): MIT)	7a. NAME OF MONITORING ORGANIZATION: U.S. Air Force Office of Scientific Research
6c. ADDRESS (City, State and ZIP Code): 77 Massachusetts Avenue Cambridge, MA 02139	7b. ADDRESS (City, State and ZIP Code): Bolling Air Force Base Washington DC 20332
8a. NAME OF FUNDING/SPONSORING ORGANIZATION: AFOSR/NA (8b. OFFICE SYMBOL (If applicable): AFOSR/NA)	9. PROCUREMENT INSTRUMENT IDENTIFICATION NUMBER: AFOSR-82-0320
8c. ADDRESS (City, State and ZIP Code): Building 410 Bolling AFB, DC 20332	10. SOURCE OF FUNDING NOS.

PROGRAM ELEMENT NO.	PROJECT NO.	TASK NO.	WORK UNIT NO.
61102F	2307	B2	

11. TITLE (Include Security Classification): See Reverse

12. PERSONAL AUTHOR(S): Bian, Theodor HH, Sifre, Pedro J., Lee, Michael

13a. TYPE OF REPORT	13b. TIME COVERED	14. DATE OF REPORT (Yr., Mo., Day)	15. PAGE COUNT
Final Report	FROM 9/1/82 TO 2/28/85	85-2-28	60

16. SUPPLEMENTARY NOTATION

17. COSATI CODES			18. SUBJECT TERMS (Continue on reverse if necessary and identify by block number)
FIELD	GROUP	SUB. GR.	Creep, Cracking, Rupture, Finite Element Analysis

19. ABSTRACT (Continue on reverse if necessary and identify by block number)

A study was made of crack initiation due to localized creep action for a nickel-base supperalloy RENE 95. Crack initiation times of single-edge-notched specimens and circumferentially notched axisymmetric specimens were determined experimentally under constant loads and a given elevated temperature. Corresponding finite element analyses using assumed stress hybrid elements were made to determine the stress and strain histories up to the crack initiation times. Through the study of specimens with notches of different geometries at different loading levels a large range of stress and strain parameters were covered. It has been found that the only parameter that falls on a narrow band when plotted against the initiation time is the magnitude of maximum equivalent stress at the time of crack initiation.

20. DISTRIBUTION/AVAILABILITY OF ABSTRACT	21. ABSTRACT SECURITY CLASSIFICATION
UNCLASSIFIED/UNLIMITED ☒ SAME AS RPT. ☐ DTIC USERS ☐	UNCLASSIFIED

22a. NAME OF RESPONSIBLE INDIVIDUAL	22b. TELEPHONE NUMBER (Include Area Code)	22c. OFFICE SYMBOL
DAVID GLASGOW, MAJOR, USAF	(202) 767-4937	AFOSR/NA

DD FORM 1473, 83 APR — EDITION OF 1 JAN 73 IS OBSOLETE.

SECURITY CLASSIFICATION OF THIS PAGE

11. TITLE (Include Security Classification)

"Finite Element andExperimental Studies of Creep Crack Initiation of RENE-95 Superalloy"

ACKNOWLEDGEMENT

The research program reported here was conducted under the Air Force Program for Research on Aircraft Propulsion Technology (AFRAPT). Professor R.M.N. Pelloux of the Department of Materials Science and Engineering, M.I.T. was an advisor. We also received helpful advise from many of Professor Pelloux's students in particularly Dr. Kenneth Bain and Mr. Yiannis Vasatis. Major David Glasgow of AFOSR was the technical monitor of the program.

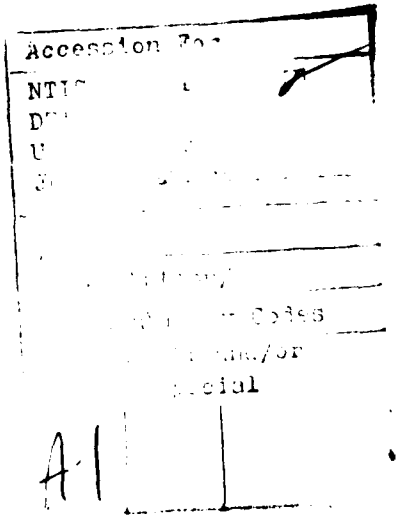

ABSTRACT

An attempt has been made to find a parameter that can be used to correlate the crack initiation due to localized creep action for a nickel-base superalloy RENE 95. The study consists of combined experimental investigations and finite element analyses. Creep crack initiations of single-edge-notched specimens and circumferentially notched axisymmetric specimens were determined experimentally under constant loads and a given elevated temperature. Corresponding finite element analyses using asumed stress hybrid elements are made to determine the stress and strain histories up to the crack initiation times. Through the study of four different geometries for the single-edge-notched specimens and both U-shaped and V-shaped notch for the axisymmetric specimens at different loading levels a large range of stress and strain parameters are covered. It has been found that the only parameter that falls on a narrow band when plotted against the initiation time is the magnitude of maximum equivalent stresses at the time of crack initiation.

TABLE OF CONTENTS

1. INTRODUCTION

One of the important considerations for life prediction of gas-turbine engine structures is fracture under high temperature creep conditions. The process for crack fracture may be divided into creep crack initiation and crack propagation. Research studies on creep rupture have been concentrated on the pheonomena of crack propagation and on damage due to large strains in tertiary creep. For such materials it is most important to establish a method for estimating the time for creep crack initiation under creep condition.

The objective of the present research program is to obtain a criterion for creep-crack initiation through a combined analytical and experimental investigation of typical gas-turbine materials. For a notched specimen under applied load and at elevated temperature, the time histories of the state of stresses and strains at the root of the notch can be calculated by using the finite element method. The crack-initiation time can be determined from an experiment. Then through a correlation between analyses and tests of specimens of different notch geometries and under different loadings, it is expected that some rules can be established for the estimation of the crack initiation time under elevated temperature creep conditions.

Many alloys used for blades and disks of gas-turbine engines are creep brittle materials. This is to say that at the time of creep crack initiation the magnitude of total strain at the crack region is of the order of only a few percent. For this problem, a finite element analysis using small deformation theory is adequate.

This research study was accomplished through the two graduate thesis works by Pedro J. Sifre and Michael J. Lee. The details of the

experimental program and numerical analysis as well the results of their correlation have been documented in their theses [1,2]. The present document is the final report of this research program. Only high lights in Reference 1 and 2 are presented but the results of the present research study are discussed in details.

Section 2 is a review of existing research studies of creep behavior of notched specimens and the decision made in choosing for the present investigation the goemetries of the notches and the loading magnitude for both single-edge-notched (SEN) and axisymmetrically notched specimens made of RENE-95 super-alloy. A description of the experimental technique for detecting the crack initiation is also given.

Section 3 is a brief description of the finite element method used to analyze the elastic-plastic and creep behaviors. For the former a viscoplastic theory in conjunction with a mechanical sub-element (sub-layer) model is used.

Section 4 presents the results by the experimental program and by the finite element solutions obtained for the test cases up to the crack initiation times that are determined from the experimental program. The results are synthesized and presented in the form of relations between certain stress and strain parameters and the crack initiation time.

Conclusions obtained by these correlation studies are given in Section 5.

2. REVIEW OF RELATED RESEARCH STUDIES AND SELECTION OF NOTCHED SPECIMENS FOR CREEP TESTING

Many researchers have studied creep behavior under multiaxial states of stress by testing notched specimens [3-7]. Their focus was on creep rupture for long period of time when the stationary-state conditions for stress distributions have been reached. The question to be answered were the deformation and rupture behaviors in the tertiary creep stage under multiaxial state of stress. In such cases the creep damage extends across the entire cross section of the test specimen. Hayhurst and his colleagues used finite element method to obtain stress distribution in their test specimens [4,5].

Under the supervision of Professor A. Pineau of the Ecole des Mines de Paris, an intensive study of creep damage for strainless steel was conducted by Mudry [8]. The investigation involves creep tests of round bars with circumferential notches that yield low values of stress gradient such that the creep damage extends across the entire cross section. The specimens can then be sliced and examined under microscope at different stages of damage. This study is also a combined finite element analysis and experimental investigation in an attempt to determine the effects of stress and strain on creep damage. For stainless steel it has been established that both stresses and strains are governing factors for creep damage. Here the damage is a measurement of the density of grain-boundary cracks. However, it is still required in establish the critical value of such damage parameters that will result to rapid crack growth under creep conditions.

Another important conclusion in Professor Pineau's study is that consistent relations between damage and stresses and strains can be maintained only when the creep strains are sufficiently small such that the tertiary creep effects need not be considered inthe constitutive equations.

A combined experimental numerical procedure has been used by Hinnerichs et al to determine the creep crack growth rate for center cracked plate specimens of IN-100 superalloy [9].

Studies of creep crack propagation and rupture of notched specimens of gas turbine materials have also been conducted at M.I.T. by McCabe [10] and Bain [11]. The specimens used were RENE-95 Superalloy. They are specimens of rectangular cross-section with single-edged U-shaped notches.

Creep crack growth tests of single-edged notch (SEN) specimens of width equal to 11.68 mm and thickness equal to 4.45 mm and notch depths between 0.6 and 1.8 mm and root radius of about 0.05 mm were made at two different temperatures.

Their conclusions are:

(1) Under constant applied load the period between creep crack initiation and creep rupture took, typically, only 1% to 10% of the life of the specimen. Thus, for this type of notched speciments the time to failure can be considered as an approximate measurement of the crack initiation time.

(2) An equivalent stress intensity factor K_I can be calculated by assuming the notches as sharp notches. The tests indicate that the time to failure, hence also the creep crack initiation time varies inversely as the fourth power of K_I.

Since, for the super-alloy REN-95 some experimental studies for crack growth have already been made at M.I.T. and data on its mechanical properties have already been collected, it was decided to choose RENE-95 again for the present investigation of creep crack initiation. RENE-95 is a creep brittle material for which the creep strains at the root of a notch at the crack initiation time are limited to small strain range. The notch geometries and stress ranges will be chosen such that total strain at the notch will remain small so that the corresponding finite element solutions can be limited only to small strains. In that case, in the finite element method the same global elastic stiffness matrix of the entire solid can be used for each of the incremental solutions. Thus the computing effort would not be overly excessive.

For this research program it was decided to follow the earlier works at M.I.T. [10,11] to use SEN specimens with notch radii much smaller than the thickness. In such case the state of stress near the notch would be essentially plane strain state, hence for the corresponding numerical solution it was also assumed that two-dimensional plane strain finite element analysis can be used instead of a much more time-consuming three-dimensional analysis.

It has been recognized, however, that specimens with single-edged notches are not exactly in plane-strain state. Hence, for a better coverage of the present experimental-finite element correlation, axisymmetric specimens of two different notch geometries are included.

To determine creep crack initiation times, tests were conducted at various stress level for the two types of specimens for different notch geometries.

As shown in Figure 1, the SEN specimen has a gage length of 25.4 mm, a width of 11.7 mm and a thickness of 4.45 mm. Notches were cut into the specimen with three different root radii: 0.063 mm, 0.20 mm and 0.50 mm. For the smallest root radius, three different notch depth were cut. The actual radiis r at the root of the cut for the different notch depth d are

d (mm)	r (actual)
0.5	0.063 mm
1.0	0.061 mm
2.0	0.055 mm

For the specimens of root radii of 0.20 and 0.50 mm the notch depths were all 1 mm.

For the axisymmetric specimens, circumferential U-notches and V-notches were used. The goemetries of the specimens and the notches are shown in Figure 2.

Forty-seven SEN specimens and twenty axisymmetric specimens were tested under different values of constant loads and at constant temperature of 650°C. These leads to a large spectrum of stress and strain distributions and histories.

Of the 47 SEN specimens 37 were tested in air while 10 specimens were tested with a retort consisting of high purity argon environment. All axisymmetric specimens were tested in air.

All creep tests were conducted under constant applied load. The appearance of crack initiation were monitored by the D.C. potential drop technique [12]. The change in potential field on a current carrying body caused by the formation of a crack can be measured. Figure 3 is a schematic

representation of the equipment used for detecting a crack of a SEN specimen. The leads that are attached to record the potential are positioned on two sides of the mouth of the notch. Both theoretical solutions and experimental calibrations are available to establish the relation between the change in potential and crack extension for plane specimens such as the SEN specimen. A crack length of the order of 100 microns have been shown to be detectable [13,14].

For axisymmetric specimens, however neither theoretical nor experimental results were available prior to the present research program. The complication, of course, is due to the fact that the circumferential position of the crack site is not known apriori. Using an equipment same as that for SEN specimen one always found that whenever a noticable potentical drop was detected, rupture of the specimen followed almost immediately. Recently Vasatis [15] of the Materials Science and Engineering Department at M.I.T. has perfected a new D.C. Potential drop system to read with high precision the voltage variation across two leads that are positioned on two sides of the circumferential notch due the existence of a crack at the root of the notch. The sensitivity of the measurement is dependent on the relative locations of the crack and the leads, but the crack initiation can be detected with certainty. From an experiment made on a V-notched axisymmetric specimen made of RENE-95 it was shown that over 95% of the creep rupture life is used up before any significant potential change can be detected. As a result it is concluded for the present axisymmetric RENE 95 specimens, creep crack initiation times are considered as the same as the rupture time.

3. DEVELOPMENT OF COMPUTER PROGRAMS FOR COMBINED ELASTIC-PLASTIC AND CREEP ANALYSES

The basic approach in the present investigation is to conduct creep tests of specimens of different notch geometries under different applied loads to determine the crack initiation times in each case. Then by using a finite element program the histories of stresses and strains near the root of the notches can be obtained. Such informations as creep strains at crack initiation and variation of maximum stresses near the root of the notch can then be determined. An attempt is then made to establish a criterion for estimating the crack initiation time.

A finite element program based on assumed stress approach was developed for analyzing creep and viscoplastic behavior of solids [16]. The method was used for the analysis of plane stress problems of elastic-plastic materials using mechanical sub-layer model [17]. It has also been used for analyzing creep problems [16]. The key features of the method is that although this is a material nonlinear problem only linear elastic stiffness matrix is required in the incremental solution. The hybrid elements have been shown to yield better accuracy than that by conventional elements.

As indicated in Section 2 for the SEN specimens, the finite element analyses are based on plane strain assumption. For simplicity only 4-node and 8-DOF plane strain elements are used. Initially elements derived by using seven assumed stress parameters (7-β) are used [16,17]. During this research period a new 4-node plane element was developed at the M.I.T. Aeroelastic and Structures Research Laboratory. The new element [18] is based on only five independent stress parameters and has been demonstrated to be less sensitive to element distortions. The latter is incorporated in the present

program. For the axisymmetric solids the elements are the four-node and 8-DOF elements derived by Spilker [19]. Another important improvement of this computer program is to incorporate and efficient automatic mesh generation routine for the finite element analyses.

3.1 Rheological Model Used in Present Analyses

For the elastic-plastic behavior, a mechanical subelement model is used to represent the time independent stress strain relation [17]. For RENE-95 material, the transient creep constitutes less than 5% of the total creep strain for the time period significant in our investigation. Thus, the creep behavior is assumed to be entirely in steady state creep (or secondary creep) with the strain rate determined by a power law. The rheological model used is shown in Figure 4. The total strain ε is given by:

$$\varepsilon = \varepsilon^e + \varepsilon^p + \varepsilon^c \tag{3.1}$$

where ε^e, ε^p and ε^c are respectively elastic, plastic and creep strains.

The mechanical subelement model consists of equally strained elastic-perfectly-plastic subelements in parallel. All elements have the same elastic modulus but with different yield limits. Under such model a uniaxial stress-strain curve is represented by one with piecewise linear segments as shown in Figure 5.

Let the tangent modulus of this i^{th} segment by E_i, then the ratio of the area A_i of the i^{th} subelement to the total area A is given by:

$$\frac{A_i}{A} = \frac{E_i - E_{i+1}}{E_1} \tag{3.2}$$

A model of N sublelement would have N-1 elastic-plastic elements and one elastic elements are shown in Figure 4.

The elastic-perfectly-plastic behavior of each subelement is represented by a visco-plastic element shown by a damper and a slider in parallel which are then connected in series with a linear spring. For multi-axial stress conditions the components of plastic strain rate is given by

$$\dot{\varepsilon}^{vp} = \gamma \langle \phi \rangle \frac{\partial F}{\partial \underset{\sim}{\sigma}} \tag{3.3}$$

where

$F(\underset{\sim}{\sigma}) = 0$ represents the yield surface

$$\text{and} \quad \langle \phi \rangle = \begin{cases} \bar{\sigma} - \sigma_y & \text{for } \sigma > \sigma_y \\ 0 & \text{for } \sigma \leq \sigma_y \end{cases} \tag{3.4}$$

with $\bar{\sigma}$ = equivalent stress under multiaxial conditions (in this case Mises-Hencky condition

σ_y = yield stress by the subelement model

γ = arbitrary fluidity-parameter

As each layer accumulates plastic strains, the stress in each layer relaxes. When an equilibrium state is reached, the equivalent stress $\bar{\sigma}$ in each sublayer, except the elastic layer, must be equal to its yield stress. Such state can be reached by successive finite element analyses using initial strains determined by the above equation. To obtain a stable finite element solution the increment of ficticious time is limited to [21]

$$\Delta t \leq \frac{4(1+\nu)}{3E\gamma} \tag{3.5}$$

where ν = Poisson's ratio

E = Elastic constant

As shown in Figure 4, the total strain which consists of elastic and plastic strains can be obtained from the visco elastic analysis and the stress components can be determined by

$$\sigma_{ij} = \sum_{n=1}^{N} \frac{A_n}{A} \sigma_{ijn} \tag{3.6}$$

The time independent elastic-plastic solution is, thus accomplished through a creep analysis program using the initial strain approach.

A finite element solution for initial strain involves the determination of redistribution of stress and strain due to prescribed components of initial strain increments in each element. For the assumed stress hybrid method the procedure has been outlined in Ref. [20]. Basically the effect of initial strain is represented by equivalent nodal loads. A routine finite element solution using the original global elastic stiffness matrix can be made to obtain the stress and strain increments.

3.2 Procedure for Creep Analysis

For materials with only steady creep behavior, at a given time with the state of stress known the components of creep strain rate can be determined by

$$\dot{\varepsilon}_y^c = f(\bar{\sigma}) \frac{\partial F}{\partial \sigma_{ij}} \tag{3.7}$$

where $\bar{\sigma}$ is the equivalent strain.

$F(\sigma_{ij}) = 0$ is the yield condition.

and $f(\bar{\sigma})$ defines the relation between strain rates and stresses. For the next time increment Δt the creep strain which may be considered as initial strain for this time increment is given by

$$\Delta \varepsilon_{ij}^{c} = \dot{\varepsilon}_{ij}^{c} \Delta t \tag{3.8}$$

In the finite element solution the initial strains at the Gaussian stations for each element are determined and the stress increments at these stations are obtained by an initial strain finite element analysis. The states of stress are then updated and solutions for the next time increments are obtained. This is a general time marching procedure that has been used by many authors [22,23]. To insure the procedure to be stable the time interval Δt must be limited to a value for which the creep strain increment in that interval at the point of greatest equivalent total strain is less than some small fraction of the total strain at t=0 [24]. For this analysis such fraction is taken as 0.9%. Because creep strain rate decreases with time the time interval Δt for the creep analysis may be increased gradually with time. Another criterion that has been introduced is that the ratio between two successive time increment should be less than 1.35.

At the end of each interval the equivalent stresses at the Gaussian points are checked. In general, further plastic deformation may be developed in some elements, and a time-independent elastic-plastic analysis should be performed.

Equations (3.3) and (3.7) are, in fact, based on the flow rule in plasticity, i.e. the components of strain rates $\dot{\varepsilon}_{ij}$, which may be either $\dot{\varepsilon}^{vp}_{ij}$ or $\dot{\varepsilon}^{c}_{ij}$, are given by

$$\dot{\varepsilon}_{ij} = \frac{3}{2}\frac{\dot{\bar{\varepsilon}}}{\bar{\sigma}} S_{ij} \tag{3.9}$$

where $\dot{\bar{\varepsilon}}$ = equivalent strain rate

$\bar{\sigma}$ = equivalent stress

S_{ij} = deviatoric stress

For axisymmetric solids these strain components are

$$\begin{aligned}
\dot{\varepsilon}_r &= \frac{\dot{\bar{\varepsilon}}}{2\bar{\sigma}}(2\sigma_r - \sigma_\theta - \sigma_z) \\
\dot{\varepsilon}_\theta &= \frac{\dot{\bar{\varepsilon}}}{2\bar{\sigma}}(2\sigma_\theta - \sigma_r - \sigma_z) \\
\dot{\varepsilon}_z &= \frac{\dot{\bar{\varepsilon}}}{2\bar{\sigma}}(2\sigma_z - \sigma_r - \sigma_\theta) \\
\dot{\gamma}_{rz} &= \frac{3\dot{\bar{\varepsilon}}}{\bar{\sigma}}\sigma_{rz}
\end{aligned} \tag{3.10}$$

where $\bar{\sigma} = [\frac{1}{2}\{(\sigma_r-\sigma_\theta)^2 + (\sigma_\theta-\sigma_z)^2 + (\sigma_z-\sigma_r)^2\} + 3\sigma_{rz}^2]^{1/2}$ (3.11)

For the plane strain problem, the non-zero stress components are σ_x σ_y σ_z and σ_{xy}. However, σ_z is not independent on account of the plane strain condition $\varepsilon^e_z + \varepsilon^p_z = 0$. By using the Prandtl-Reuss relation the three independent strain components, are

$$\dot{\varepsilon}_x = \frac{\bar{\dot{\varepsilon}}}{\bar{\sigma}} [(1-\tfrac{1}{2}\nu)\sigma_x - \tfrac{1}{2}(1+\nu)\sigma_y - (\tfrac{1}{2}-\nu)\sigma_z]$$

$$\dot{\varepsilon}_y = \frac{\bar{\dot{\varepsilon}}}{\bar{\sigma}} [(1-\tfrac{1}{2}\nu)\sigma_y - \tfrac{1}{2}(1+\nu)\sigma_x - (\tfrac{1}{2}-\nu)\sigma_z]$$

$$\dot{\gamma}_{xz} = \frac{3\bar{\dot{\varepsilon}}}{\bar{\sigma}} \sigma_{xy} \qquad (3.12)$$

where $$\bar{\sigma} = [\tfrac{1}{2}\{(\sigma_x-\sigma_y)^2 + (\sigma_y-\sigma_z)^2 + (\sigma_z-\sigma_x)^2\} + 3\sigma_{xy}^2]^{1/2} \qquad (3.13)$$

3.3 Accuracies of the Finite Element Solutions

To check the accuracies of and to determine the appropriate mesh size for the finite element solutions, a doubled-edge-notched specimen were analyzed using a coarse mesh with 169 4-node elements and 398 D.O.F. and a fine mesh with 404 elements and 900 D.O.F. for one quarter of the solid using the 7-β element. The elastic stress concentration factor k_t based on the stress at a point near the root of the notch are 9.71 and 9.98 respectively for these two meshes. The analytical solution given by Reference 25 is 10.02. When the new 5-β elements are used the corresponding value obtained by using a coarse mesh the factor k_t is 9.73. This indicates that for the present problem the finite element solutions by the coarse mesh is only about 2.5% off and solutions by both the 7-β and 5-β solutions are acceptable.

The creep behavior of a round specimen with circumferential notch of British Standard V-shape was determined by Hayhurst and Henderson using the finite element method. [4] The same problem was analyzed by the present program. A comparison of the normal stress σ_y distributions along the radius at minimum section is shown in Figure 6. The agreement of the two results is very good. This is another indication that the present method can provide acceptable accuracy.

4. FINITE ELEMENT SOLUTIONS AND CORRELATION WITH EXISTING EXPERIMENTAL RESULTS

In the experimental investigation specimens of single-edged notches were used. However, finite element solutions for elastic stress distributions near the root of both single-edged notch and double-edged notch have been found to be undistinguishable. Thus, in the future element solutions the specimens are all considered as double-edge notched, and it is only required to analyze one-quarter of the specimen.

The elastic-plastic behavior for RENE-95 at 650°C obtained from a test of a standard tension specimen is given as:

$$\varepsilon^p = 6.9 \times 10^{-5} \left(\frac{\sigma}{1000}\right)^{17.61} \tag{4.1}$$

This relation is approximated by a curve with four piece-wise linear segments. The stresses σ_y and strains ε_y at the ends of the first three linear segments are given as follows:

End of Segments i	σ_y(?a)	ε_y
1	1151	0.0065
2	1236	0.009
3	1330	0.015

For the corresponding multi-layer model (Figure 5b), the layer yield stresses σ_y^i ($=E\,\varepsilon_y^i$) of the three layers are respectively 1151, 1584 and 2610 MPa while the fourth layer is elastic. The area ratios of the four layers are:

$$\rho_1 = \frac{A_1}{A} = \frac{E_1 - E_2}{E_1} = 0.8040$$

$$\rho_2 = \frac{A_2}{A} = \frac{E_2 - E_3}{E_1} = 0.1044$$

$$\rho_3 = \frac{A_3}{A} = \frac{E_3 - E_4}{E_1} = 0.0816$$

$$\rho_4 = \frac{A_4}{A} = \frac{E_4 - E_5}{E_1} = 0.010$$

The steady-state creep behavior for RENE-95 at 650°C were obtained by testing of smooth tensile specimens using a A.T.S. lever arm tester. Steady-state strain rates were determined at various stress levels. The resulting creep strain rate vs stress relation in the form of the Norton-Bailey power relation is given by:

$$\dot{\varepsilon}^c = 5.689 \times 10^{-8} \left(\frac{\sigma}{1000}\right)^{29.12}$$

The experimental data for the 47 SEN specimen and 20 axisymmetric specimens are given in Table 1 and 2 respectively. It is noted that the applied loads chosen for the creep test were high enough such that. In most cases creep crack initiations occurs within a day with only a few case extended to a few hundred hours. For several tests which run over that length of time without any sign of crack initiation creep tests were terminated. The restriction of the creep test times was applied mainly because of the limitation in time for the present project and the limitation in fund for finite element solutions. It turns out that because the time to crack initiation were short, the stress redistribution across the minimum cross section in each case never reached the stationary state and creep strain was developed only in narrow zones near the root of the

notch. For the first few specimens tested the root radius were of the smallest or around 0.06 mm. In order to simulate the triaxiality condition typical of plane strain conditions, side grooves were cut on both sides of the specimens. Inspections of the fracture surfaces of some of these specimens revealed that cracks were originated at the corner. It is possible that this was the result of the additional stress concentrations caused by the side grooves. The results of these early tests were not included in the present experimental-numerical correlation and the side grooves were omitted in all the later SEN specimens.

A quick comparison of the crack initiation times given in Table 1 reveals that there was no apparent increase in crack initial time, when tested in argon than that when tested in air. On the other hand while in air the crack initiation time usually occupies nearly the entire rupture time, the crack initiation in argon only occupies a small portion of the rupture time. The means that the rate of crack propagation is reduced considerably in argon than that in air.

Examination of fracture surface of specimens tested in argon reveals the sign of oxidation in the region close to the notch. Such contamination by oxygen is probably the result of imperfect control of the enviroment in the retort.

The test cases that involves argon were not included in the experimental-numerical correlation.

For the finite element solutions it was decided to consider only four geometry types for the SEN speciments. They are as follows:

Geometry type	root radius r (mm)	depth of notch d (mm)
1	0.061	1.0
2	0.055	2.0
3	0.200	1.0
4	0.500	1.0

A typical mesh pattern used for the plane strain solutions is shown in Figure 7. The mesh pattern used for the axisymmetric solids with U-notch and V-notch are shown respectively in Figure 8 and 9.

Some typical results of the finite analyses are given in the following figures:

Fig. 10 Normal Creep Strain Profile Along Minimum Cross-Section of U-Notched Specimen.

Fig. 11 Equivalent Creep Strain Profile Along Minimum Cross-Section of U-Notched Specimen.

Fig. 12 Equivalent Creep Strain Distribution Along Minimum Cross-Section Close to Notch Tip of a Type 4 Notch Specimen.

Fig. 13 Creep Strain History at the Notch Tip of a U-Notched Specimen.

Fig. 14 Normal Stress Profile Along Minimum Cross-Section of a V-Notched Specimen.

Fig. 15 Equivalent Stress Profile Along Minimum Cross-Section of a U-Notched Specimen.

Fig. 16 Time History of Stresses at the Notch Tip of a V-Notched Specimen.

From the resulting distributions of strains and stresses along the minimum cross sections of the specimen the following general observations can be made.

(1) For all the test cases the areas of high stress concentrations and hence also high creep strains are confined to a narrow region close to the notch tips. The magnitudes of creep strains are small enough to justify the assumptions that RENE 95 is a creep brittle material and the use of small deformation of finite element analysis.

(2) Although the maximum normal stresses occur at a distance from the notch tip, the maximum equivalent (effective) stresses occur at or very near the notch tip. Since the creep strain rate is directly related to the equivalent stress, the maximum strains also tend to occur at or very near the notch tip. These results are consistent with the results of post mortem inspections of all specimens that cracks appear to initiate at or near the notch tips.

(3) For all the test cases, crack initiation occured when the stationary states in stress distribution had not been reached along the minimum cross-section of the specimen. The present investigation, thus has been focused in an area different from that by earlier authors such as Hayhurst et al [3-7] whose interests were damage in gross creep deformation instead of local crack initiation.

The resulting values of normal and equivalent stresses and creep strains from the finite element solutions have been plotted against the logarithmic time scale to be used to find out whether certain parameter in stress or strain can be used to form a predictive creep crack initiation criterion.

The most significant parameters that may govern the crack initiation obviously are the normal and equivalent strains and stresses at the time of crack initiations. It is felt that for the strain parameter it may be more meaningful to use some averaged valued over a certain area instead

of just the maximum values. Thus for the present correlations it was decided to consider also averaged strain values over and area within certain distances from the notch tip as well as that over a creep damage process zone (CDPZ) which is defined as the area in which creep strains exceed 0.01%.

In the present report the following figures are included:

Fig. 17 Normal Creep Strain at the Notch Tip Vs. Initiation Time.

Fig. 18 Equivalent Creep Strain at the Notch Tip Vs. Initiation Time.

Fig. 19 Maximum Normal Creep Strain at Minimum Cross-Section Vs. Initiation Time.

Fig. 20 Acerage Normal Creep Strain Over 100 Micros Vs. Initiation Time.

Fig. 21 Average Normal Creep Strain Over CDPZ Vs. Initiation Time.

Fig. 22 Normal Stress at Notch Tip at Initiation Vs. Initiation Time.

Fig. 23 Maximum Normal Stress at Minimum Cross-Section at Initiation Vs. Initiation Time.

Fig. 24 Equivalent Stress at Notch Tip at Initiation Vs. Initiation Time.

Fig. 25 Maximum Equivalent Stress at Minimum Cross-Section at Initiation Vs. Initiation Time.

Fig. 26 Time History of Maximum Equivalent Stress at Minimum Cross-Section at Initiation for Test #7 of U-Notched Specimen. (σ^{∞} = 414.51 MPa, t_i = 224.9 hrs.)

From the preliminary results obtained by Sifre [1] an observation was made that, for the SEN specimens, the averaged normal creep strain over a length of 100 microns from the root of the notch provides the most uniform trend when plotted against the time of initiation. It was later found that certain corrections were necessary in those solutions.

A revised plot now also includes results obtained for the axisymmetric specimen is shown in Figure 20. It is clear from this figure that although the data points do show a general trend of increasing in strain values with increasing crack initiation time, the points are very widely scattered.

In fact, from figure 17 to 21 it can be concluded that it is not possible to form a criterion from a correlation using any of strain parameters used. The same is true for all the stress parameters used except the equivalent stress at the root of the notch and the maximum equivalent stress at the time of crack initiation as shown in Figures 24 and 25.

The data points in each of these two figures all fall in a rather narrow band. These two bands are quite close mainly because in all cases the maximum equivalent stresses occur at or very near the root of the notch. This result is very significant since it is obtained from correlation data from different type of specimens with different notch geometries.

One would think that if this relation between maximum equivalent stress and crack initiation time, indeed, applies to notches of all kind of geometry, it should also cover the uniaxial tensiles testing of smooth bar specimens. The results of two such uniaxial testing are also located on Figure 25. It is clear that for the same equivalent stress, rupture time is longer for the case of uniaxial loading. One can only conclude that the result obtained in the present investigation only applies to notched specimens for which creep behavior is confined only to a local area. Another evidence to this statement is the result on creep fracture in circumferential U-notched specimens of Nimonic 8DA material obtained by Dyson and Loveday [7]. Their tests were under long durations when the stationary conditions for stresses were maintained and the creep strain rate was uniform along the entire cross section. In terms of equivalent

stresses their results for uniaxial and multiaxial data for creep rupture times appear to be close to each other. One can image that if the present investigation is extended to creep testing under very long duration such that stationary conditions for stresses can be reached the uniaxial and multiaxial data will converge together.

The present study is, thus, an important forward step beyond the earlier investigations of creep behavior under multiaxial loading condition. Unlike notched specimens used by earlier researchers and in the present work, structural or machine parts under elevated temperature may experience creep damage only locally and not to spread over the entire cross section even in long durations. Crack initiation under multiaxial loading condition then becomes an important consideration. The present finding that the maximum equivalent stress is the most important reference parameter for creep crack initiation, thus, is extremely important.

In order to find out whether Figure 25 determined presently can be used to develop a meaningful method for predicting crack initiation, the time history of maximum equivalent stress for case #7 in Table 2 is plotted together with the present data as shown in Figure 30. For the present data a band is indicated which covers a ratio of one to two in the time scale. It is seen that the time history solution for the test case meets the band at a very sharp angle from the bottom and the predicted crack initiation time will cover a range way over one to twenty ratio.

The question of whether the maximum principal tension stress or the equivalent stress should be used as the reference stress to determine the creep rupture behavior under multiaxial loading condition has been studied by several authors [3,5,6,7]. Hayhurst [3] has found that for pure copper the maximum principal tension should be used while for pure

aluminum the equivalent stress should be used. The experiment result by Dyson and Loveday [7] also indicates that the equivalent stress should be used as the reference stress for Nimionic 80A. It appears from a comparison of Figures 23 and 25 that the equivalent stress governs the crack initiation behavior of the present material RENE 95.

5. CONCLUSIONS

1. The present research program is a new and important addition to the study of creep damage under multiaxial loading conditions. Earlier efforts were concerning problems involving stationary stress distributions with rupture originated from gross creep strain action over entire cross section of test specimens. The present study, however is focussed on problems with stress concentrations and creep strain actions confined only to local regions. The rupture process is through crack initiation and propagation.

2. For RENE 95 specimens tested at 650°C under constant loads it was found that the only parameter that can be used to define the creep crack initiation time is the maximum equivalent stress along the minimum cross section at the crack initiation time. This is consistent with creep rupture of notched specimen under stationary stress distribution because, in that case, the creep rupture time is also determined by the magnitudes of equivalent stress. The present program of creep tests of notched specimens and corresponding finite element solutions should be extended, when economically feasible, to applied loads such that crack initiation times are at least one order longer than those in the present investigations.

3. The present study is an example that combined experimental-numerical procedures are essential in pursuing materials researhc in crack initiation under creep conditions.

4. Experimental result has indicated that the change from air to argon has no noticiable effect on the creep crack initiation time although it reduces the rate of crack propagation considerably.

REFERENCES

[1] Sifre, Pedro J., "Experimental and Computational Studies of Creep Crack Initiation of RENE 95 Nickel Based Superalloy", S.M. Thesis, Dept. of Aeronautics and Astronautics, M.I.T., August 1984.

[2] Lee, Michael, J.,"Plastic and Creep Strain Analysis and Rupture Study of Notched RENE 95 Specimens", S.M. Thesis, Dept. of Mechanical Engineering, M.I.T, February 1985.

[3] Hayhurst, D.R., "Creep Rupture under Multi-Axial States of Stress", J. Mech. Phys. of Solids, Vol. 20, pp. 381-390, Pergamon Press, 1972.

[4] Hayhurst, D.R. and Handerson, J.T., "Creep Stress Redistribution in Notched Bars", Int. J. Mech. Sci., Vol. 19, pp. 133-146, 1977.

[5] Hayhurst, D.R., Dimmer, P.R. and Chernuka, M.W., "Estimate of Creep Rupture Life Time of Structure using F.E.M.", J. Mech. Phys. of Solids, Vol. 23, pp. 335, 1975.

[6] Hayhurst, D.R., Leckie, F.A. and Morrison, C.J., "Creep Rupture of Notched Bars", Proc. Royal Society, London, Series A, Vol. 360, pp. 243-264, 1978.

[7] Dyson, B.F. and Loveday, M.S., "Creep Fracture in Nimonic 80A under Triaxial Tensile Stressing", IUTAM Symposium on Creep of Structures, ed. by Hayhurst and Ponter, pp. 406-421, 1981.

[8] Murdry, F., "Etude de la Rupture Ductile et de la Rupture par clivage d'Aciers' Faiblement Allies", Universite de Technologie de Compiegne, Doctoral Thesis, March 1982.

[9] Hinnerichs, T., Nicholas, T. and Palazotto, A., "A Hybrid Experimental-Numerical Procedure for Determining Creep Crack Growth Rate", Engineering Fracture Mechanics, Vol. 16, pp. 265-277, 1982.

[10] McCabe, R., "Creep Crack Growth in Rene 95 at 650° and 760°C", S.M. Thesis, Dept. of Materials Science and Engineering, M.I.T., 1981.

[11] Bain, K.R., "Creep Crack Growth Rates of R-95 in Air and Pure Argon", S.M. Thesis, Dept. of Materials Science and Engineering, M.I.T. February 1982.

[12] Halliday, M.D. and Beevers, C.J., "The d.c. Electrical Potential Method for Crack Length Measurement", The Measurement of Crack Length and Shape during Fracture and Fatigure, C.J. Beevers et al. (ed.), Engng. Materials Advisory Service, Ltd., 1980.

[13] Siverns, M.J. and Price, A.T., "Crack Propagation under Creep Conditions in Quenched 2 1/4 Chromium, 1 Molybdenium Steel", Int. J. of Fracture, Vol. 9, No. 2, p. 199, 1973.

[14] Gordon, P. and An, H.H., "The Mechanisms of Crack Initiation and Crack Propagation in Metal Induced Embrittlement of Metals", Metall. Trans. A., Vol. 13A, p. 457, 1982.

[15] Vasatis, I. Unpublished work, M.I.T., Dept. of Materials Science & Engineering.

[16] Pian, T.H.H. and Lee, S.W., "Creep and Viscoplastic Analysis by Assumed Stress Hybrid Finite Elements", Finite Elements in Non-Linear Mechanics, ed. by P.G. Bergen et al., TAPIR (Norwegian Inst. of Tech.), Trondheim, pp. 807-822, 1978.

[17] Pian, T.H.H., "Plasticity, Visco-Plasticity and Creep of Solids by Mechanical Subelement Methods", Numerical Methods in Coupled Systems, ed. by R.W. Lewis, E. Hinton and P. Bettess; John Wiley & Sons, Inc., N.Y., N.Y., pp. 119-126, 1983.

[18] Pian, T.H.H. and Sumihara, K., "Rational Approach for Assumed Stress Finite Elements", Int. J. of Numerical Methods Engineering, Vol. 20, pp. 1685-1695, 1984.

[19] Spilker, R.L., "Improved Hybrid-Stress Axisymmetric Elements Including Behavior for Nearly Incompressible Materials", Int. J. of Numerical Methods Engineering, Vol. 17, pp. 483-501, 1981.

[20] Pian, T.H.H., "Nonlinear Creep Analysis by Assumed Stress Finite Element Methods", AIAA Journal, Vol. 12, pp. 1756-1758, 1975.

[21] Cormeau, I.C., "Numerical Stability in Quasi-Static Elasto/Visco-plasticity", Int. J. of Numerical Methods Engineering, Vol. 9, pp. 109-127, 1975.

[22] Kraus, Harry, "Creep Analysis", J. Wiley & Sons, New York 1980, p. 186.

[23] Mendelson, A., Hirschberg, M.H. and Manson, S.S., "A General Approach to the Practical Solution of Creep Problems", Trans. ASME, Vol. 81D, pp. 585-589 1959.

[24] Zienkiewicz, O.C. and Cormeau, I.C., "Viscoplasticity-Plasticity and Creep in Elastic Solids - A Unified Numerical Solution Approach", Int. J. for Numerical Methods Engineering, Vol. 8, pp. 821-845, 1974.

[25] Creager, M. and Paris, P.E., "Elastic Field Equations for Blunt Cracks with Reference to Stress Corrosion Cracking", Int. Journal of Fracture, Vol. 3, pp. 247-252 1967.

TABLE 1 EXPERIMENTAL DATA

TEST	d	r	σ^{∞}(MPa)	ENV.	t_i(hrs)	t_r(hrs)	Remarks
1	1	0.06	465	Air	5.6	6.0	
2	1	0.06	282	Air	no	no	Run to 500hr
3	1	0.06	376	Air	8.7	9.2	
4	2	0.06	282	Air	6.5	6.9	
5	1	0.06	465	Air	3.3	3.4	Same as #1
6	1	0.06	376	Air	no	no	Run to 1100hr
7	1	0.06	431	Air	28	—	Interrupted
8	2	0.06	465	Air	0.45	0.6	
9	2	0.06	431	Air	0.95	1.2	
10	2	0.06	414	Air	0.74	0.9	
11	0.5	0.06	465	Air	no	no	Run to 545hr
12	0.5	0.06	565	Air	4.6	4.83	
13	2	0.06	395	Air	1.0	1.3	
14	1	0.06	442	Air	no	no	Run to 850hr
15	2	0.06	282	Air	115	115.3	Same as 4
16	2	0.06	376	Air	2.2	2.7	
17	2	0.06	358	Air	0.5	0.7	
18	2	0.06	339	Air	9.3	9.7	
19	2	0.06	329	Air	3.6	3.8	
20	2	0.06	320	Air	0.8	0.9	
21	2	0.06	310	Air	3.4	3.5	
22	2	0.06	282	Air	66.6	66.8	Same as 4
23	2	0.06	282	Air	25.4	--	Interrupted

TABLE 1 (Continued)

TEST	d	r	σ^{∞}(MPa)	ENV.	t_i(hrs)	t_r(hrs)	Remarks
24	2	0.06	465	Air	0.3	0.4	
25	1	0.06	453	Air	1.1	1.5	
26	1	0.20	931	Air	0.0	0.0	Instantaneous
27	1	0.20	616	Air	0.10	0.1	
28	1	0.20	565	Air	0.75	0.75	
29	1	0.20	479	Air	no	no	Run to 110hr
30	1	0.20	530	Air	no	no	Run to 110hr
31	1	0.20	556	Air	1.7	1.8	
32	1	0.20	548	Air	7.8	8.0	
33	1	0.20	548	Air	1.2	1.3	Same as #32
34	1	0.50	633	Air	44.9	45.0	
35	1	0.50	642	Air	3.5	3.6	
36	1	0.50	642	Air	20.45	20.5	Same as #35
37	1	0.50	650	Air	2.05	2.07	
38	1	0.50	650	Arg	5.4	11.3	Same as #37
39	1	0.50	642	Arg	16.0	30.7	Same as #40
40	1	0.50	642	Arg	7.0	--	Interrupted
41	1	0.50	633	Arg	73.7	--	Interrupted
42	1	0.20	556	Arg	28.8	--	Interrupted
43	1	0.20	548	Arg	0.9	0.9	Same as #32
44	1	0.20	548	Arg	6.5	--	Interrupted
45	1	0.20	539	Arg	35.0	71.1	
46	1	0.06	310	Arg	4.0	18.5	
47	1	0.06	296	Arg	12.0	52.2	

TABLE 2 SUMMARY OF EXPERIMENTAL DATA FOR AXISYMMETRIC SPECIMENS

TEST NUMBER	NOTCH CASE	σ_z^∞	t_r
1	U	499.41	1.5
2	U	474.44	2.5
3	U	449.47	3.4
4	U	424.50	9.0
5	U	399.53	410+
6	U	420.754	11.1
7	U	414.51	224.9
8	U	418.257	8.0
9	U	412.014	90.6
10	U	408.269	7.1
11	V	583.687	.2
12	V	527.5	.5
13	V	449.47	2.4
14	V	424.5	2.5
15	V	399.53	8.9
16	V	387.044	5.3
17	V	362.07	1.1
18	V	399.53	1.7
19	V	362.07	7.3
20	V	312.132	1.85

+ did not break

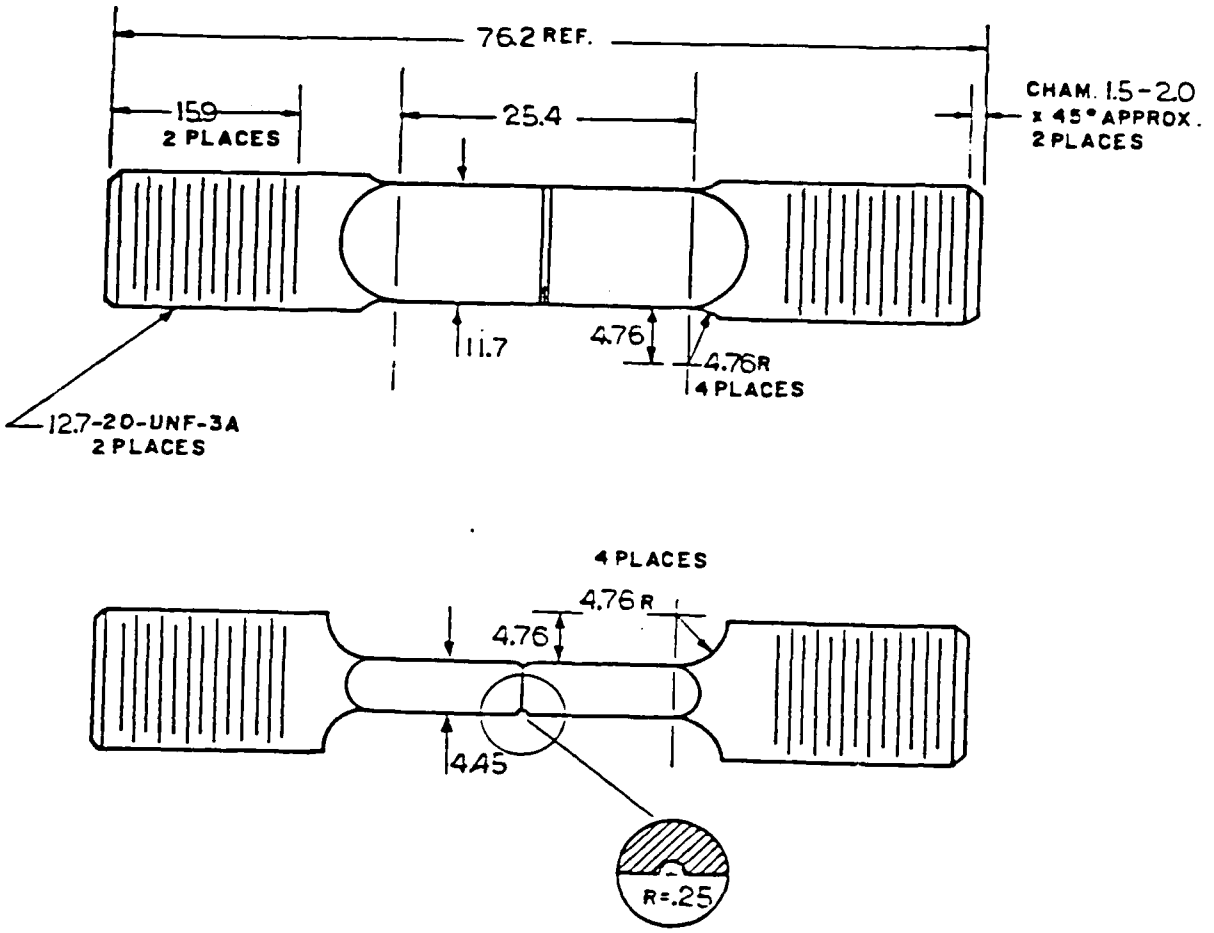

Figure 1 Single Edge Notched (SEN) Specimen Geometry (Dimension in mm) [10].

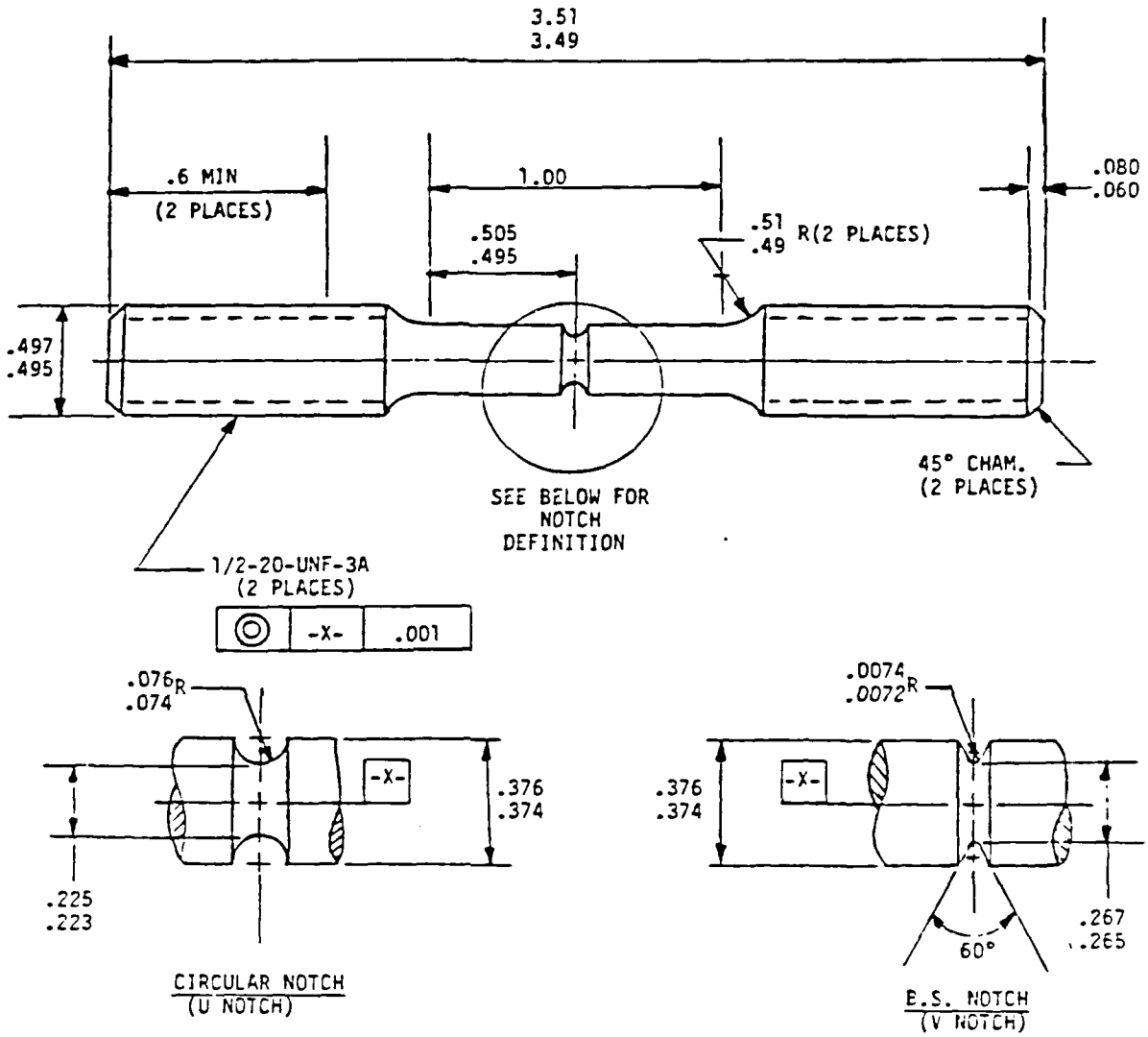

1) NOT IN SCALE.
2) ALL DIMENSIONS IN INCHES UNLESS SPECIFIED.
3) MATERIAL: P/M HIP RENE 95

Figure 2 Axisymmetric Specimens

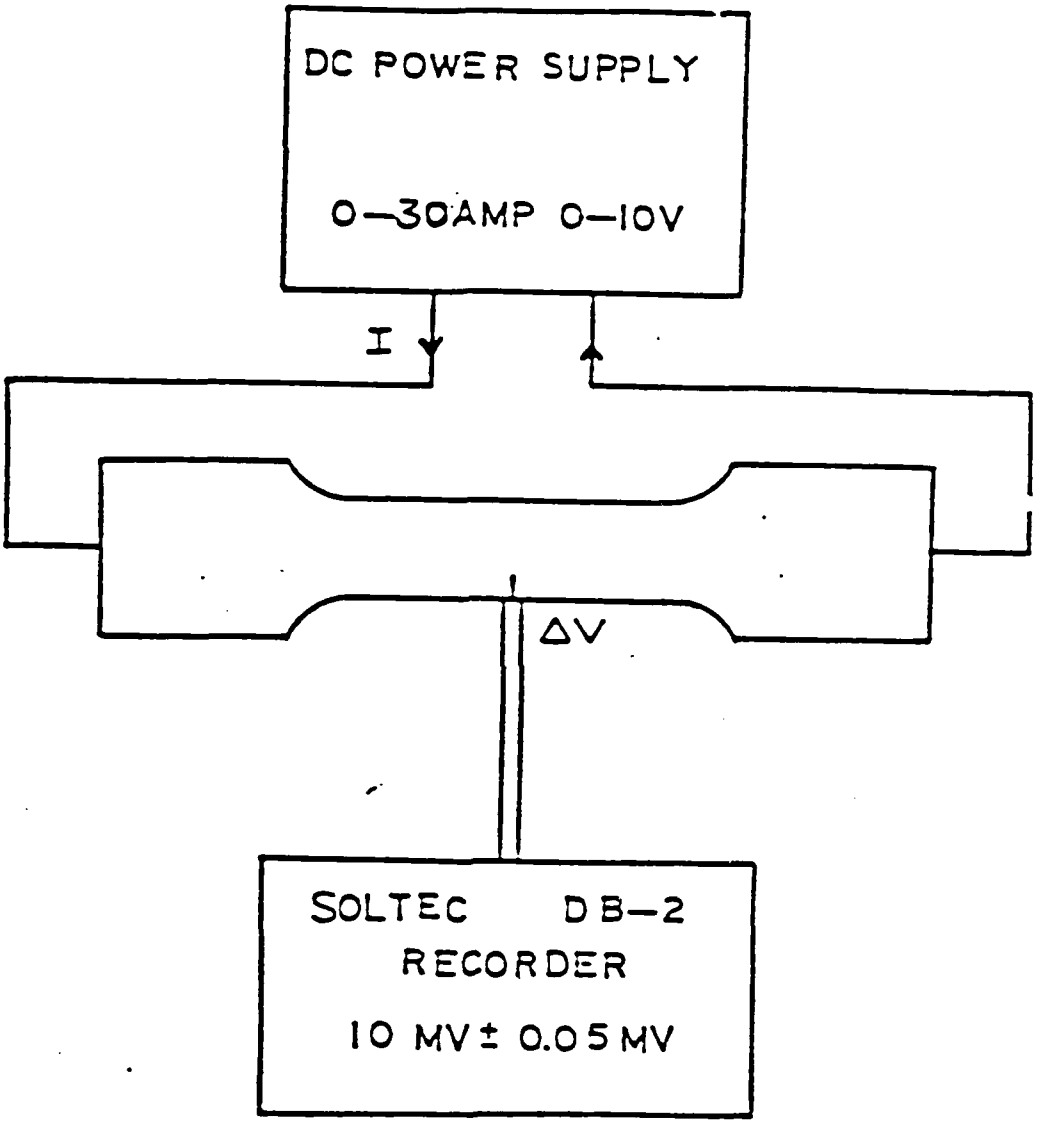

Figure 3 Schematic Diagram of D.C. Potential Drop System

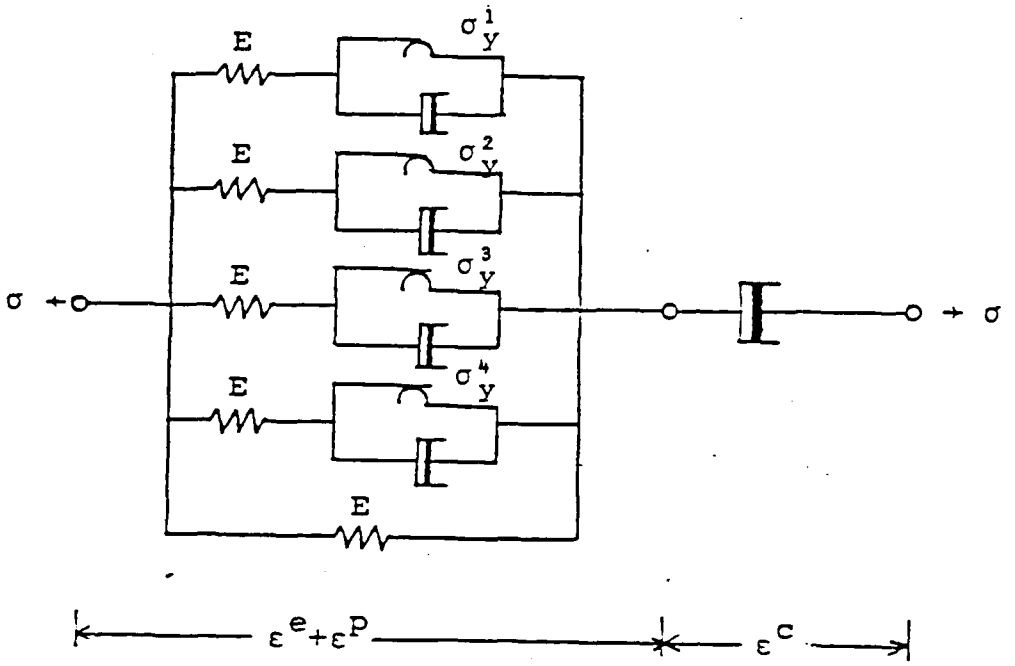

Figure 4 Rheological Model

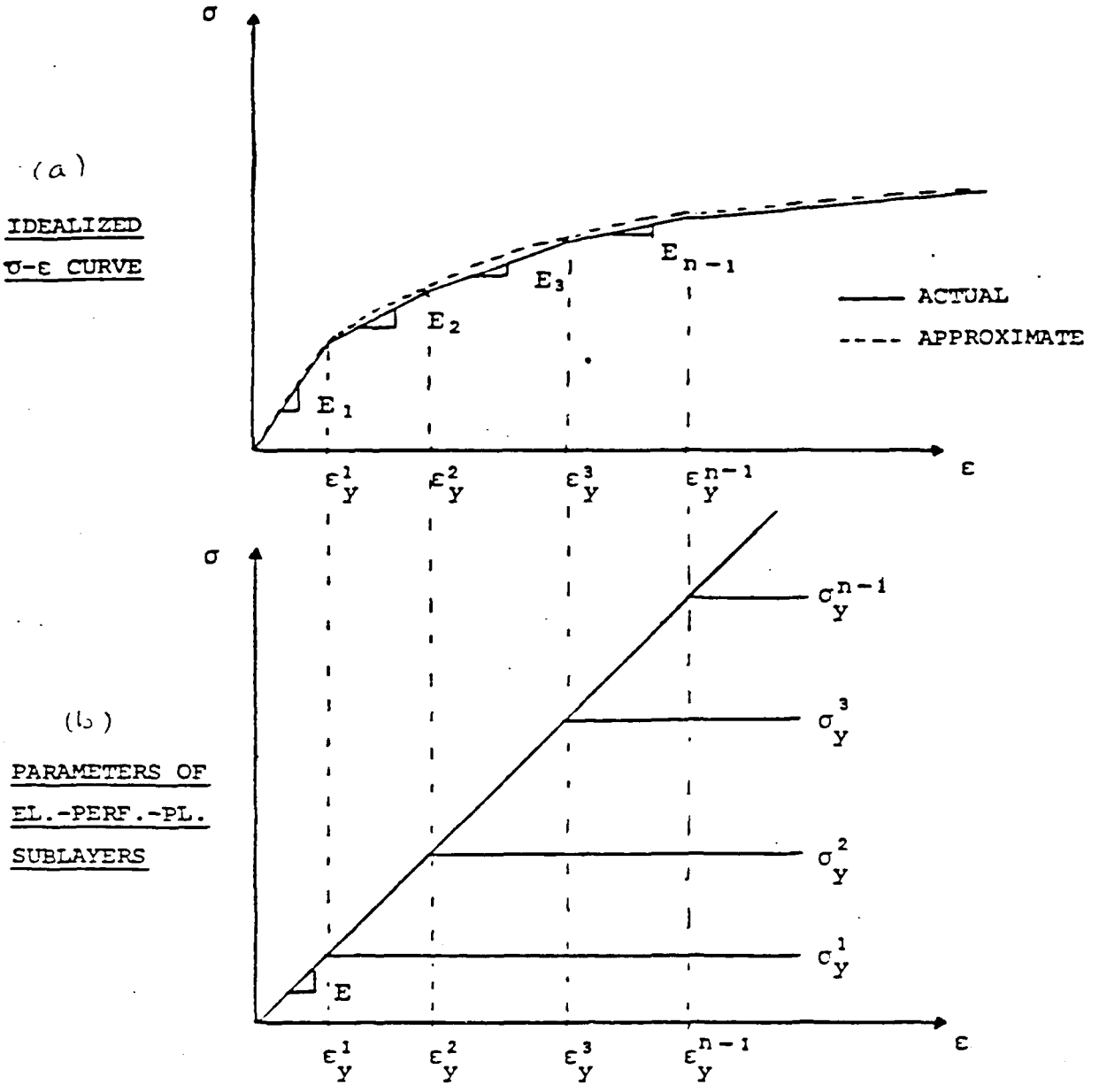

Figure 5 Mechanical Subelement Model

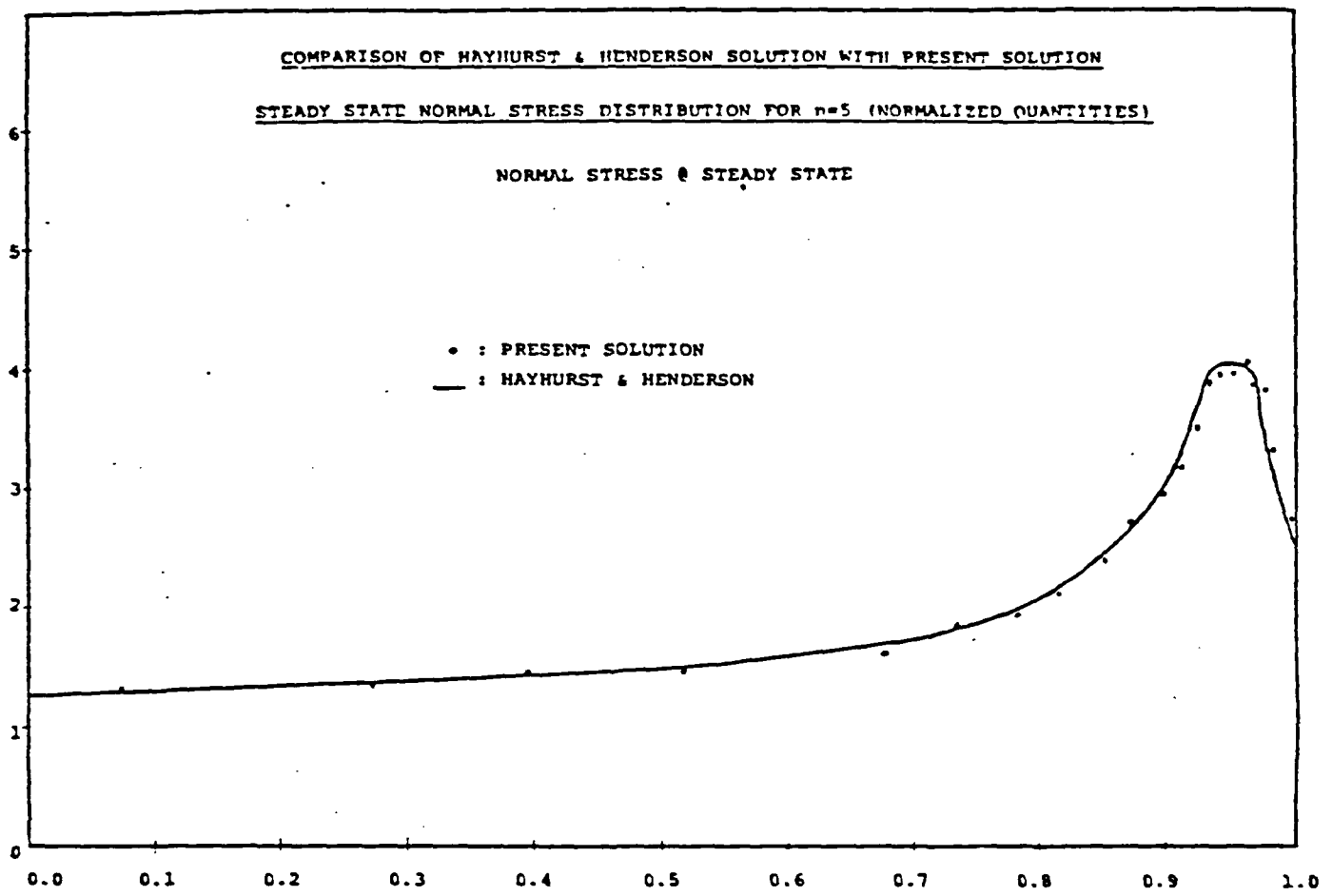
COMPARISON OF HAYHURST & HENDERSON SOLUTION WITH PRESENT SOLUTION
STEADY STATE NORMAL STRESS DISTRIBUTION FOR n=5 (NORMALIZED QUANTITIES)
NORMAL STRESS @ STEADY STATE
• : PRESENT SOLUTION
— : HAYHURST & HENDERSON
0
1
2
3
4
5
6
0.0
0.1
0.2
0.3
0.4
0.5
0.6
0.7
0.8
0.9
1.0

Figure 6

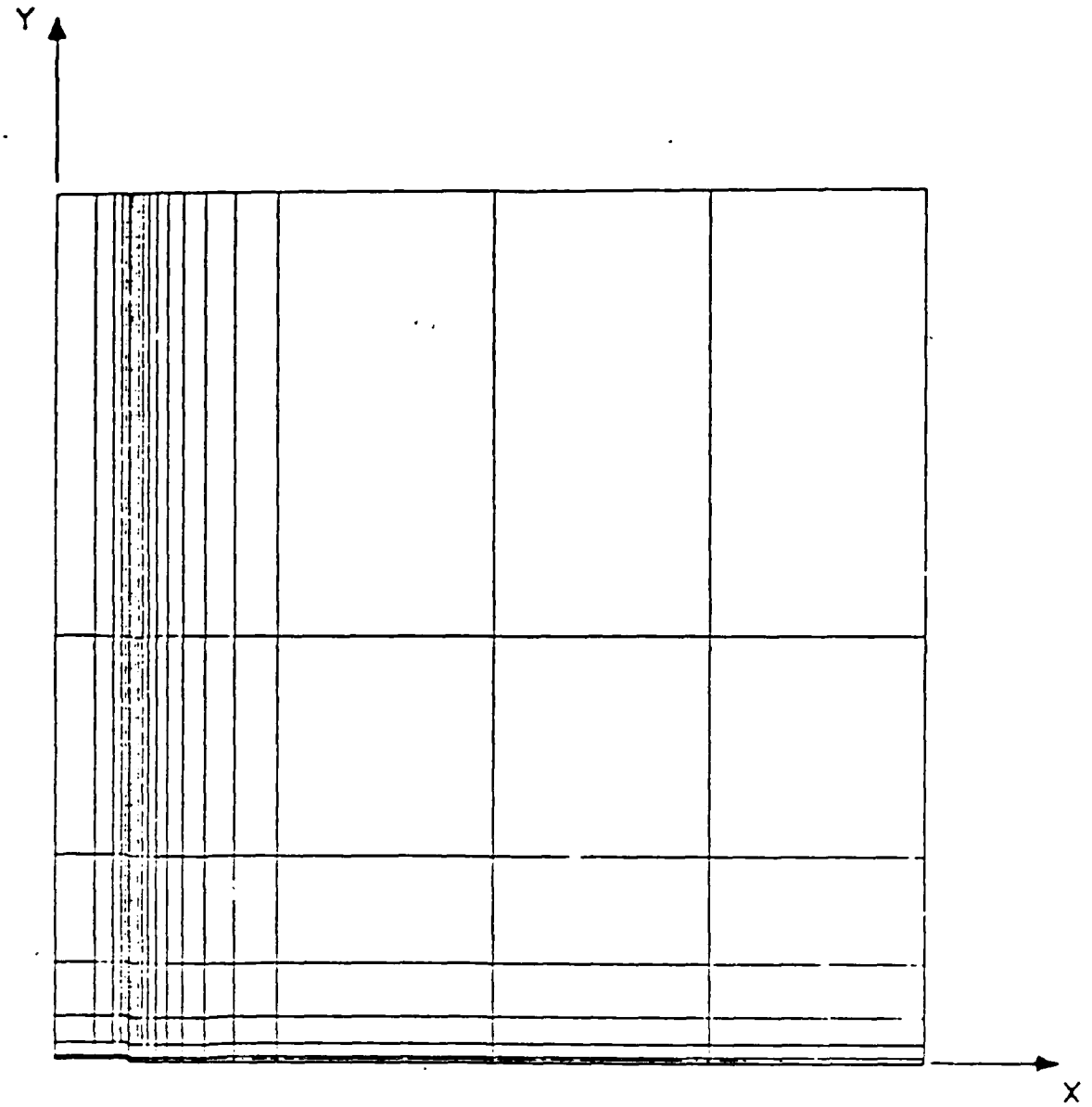

Figure 7a A Typical Mesh for Plane Strain Analysis

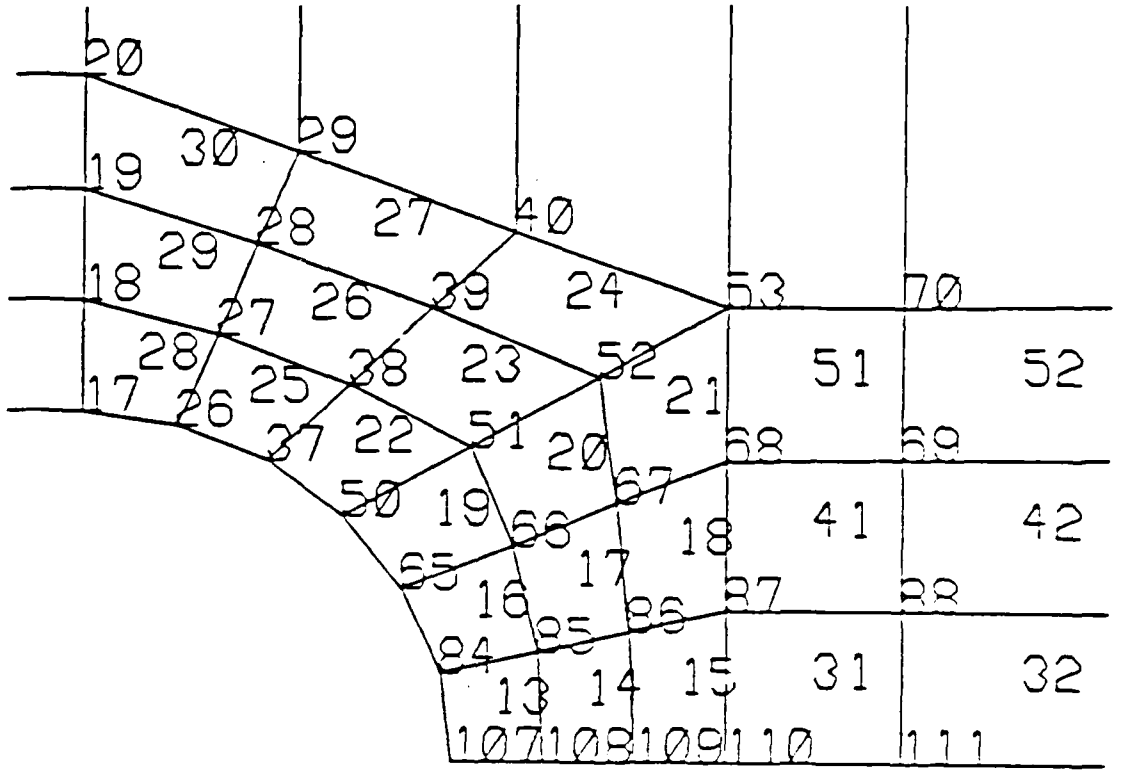

Figure 7b Mesh Arrangement Around Notch for Plane Strain Analysis

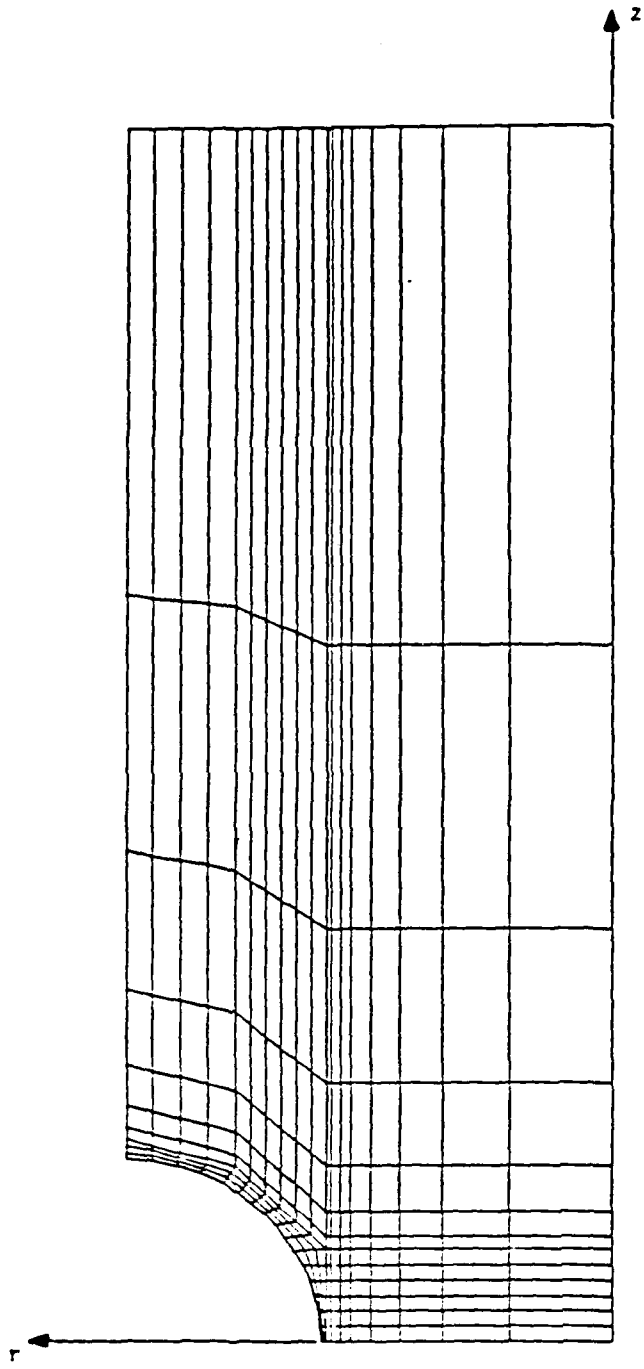

Figure 8 Mesh Used for U-Notch Analysis (222 Elements, 50 B.W., 514 D.O.F.)

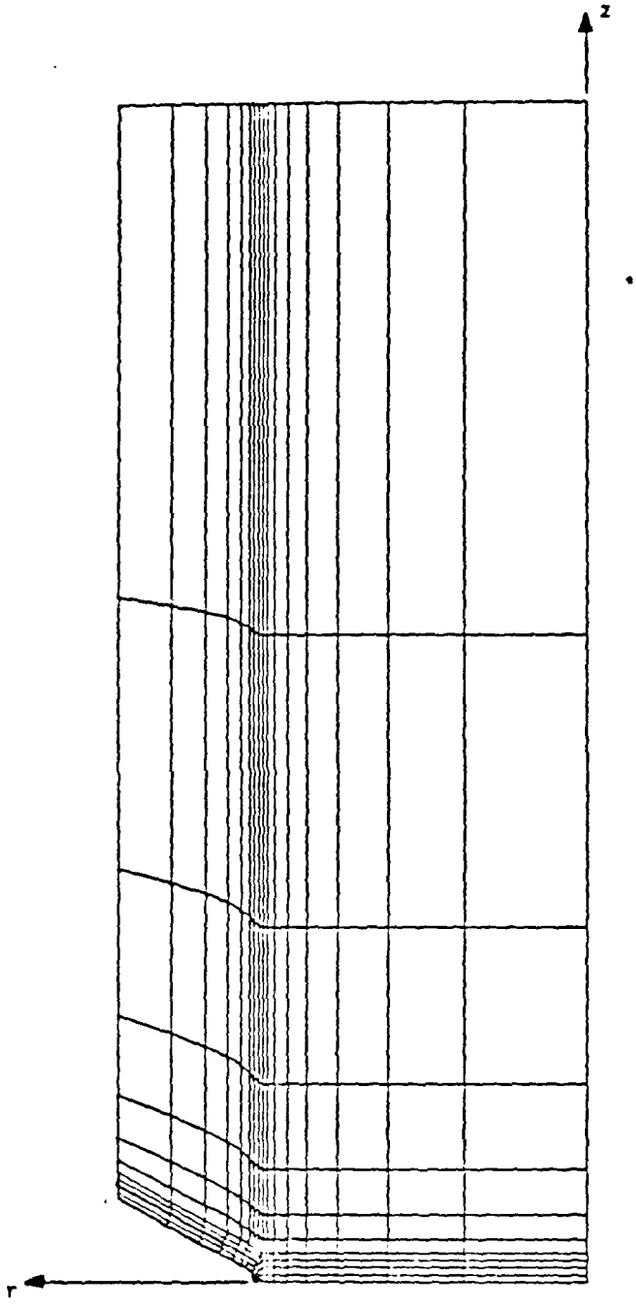

Figure 9 Mesh Used for V-Notch Analysis (192 Elements, 66 B.W. 448 D.O.F.)

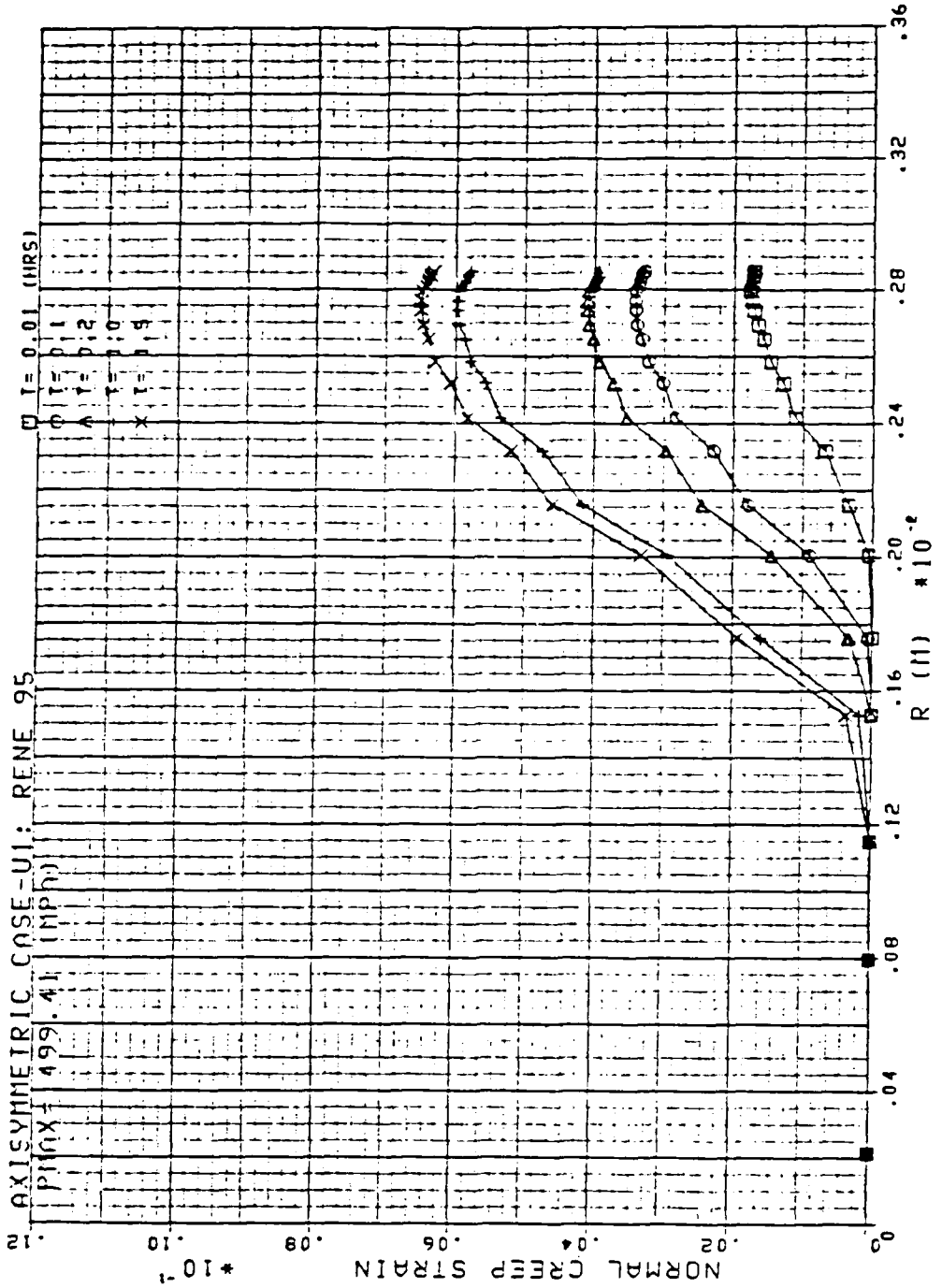

Figure 10 Normal Creep Strain Profile Along Minimum Cross-Section of U-Notched Specimen

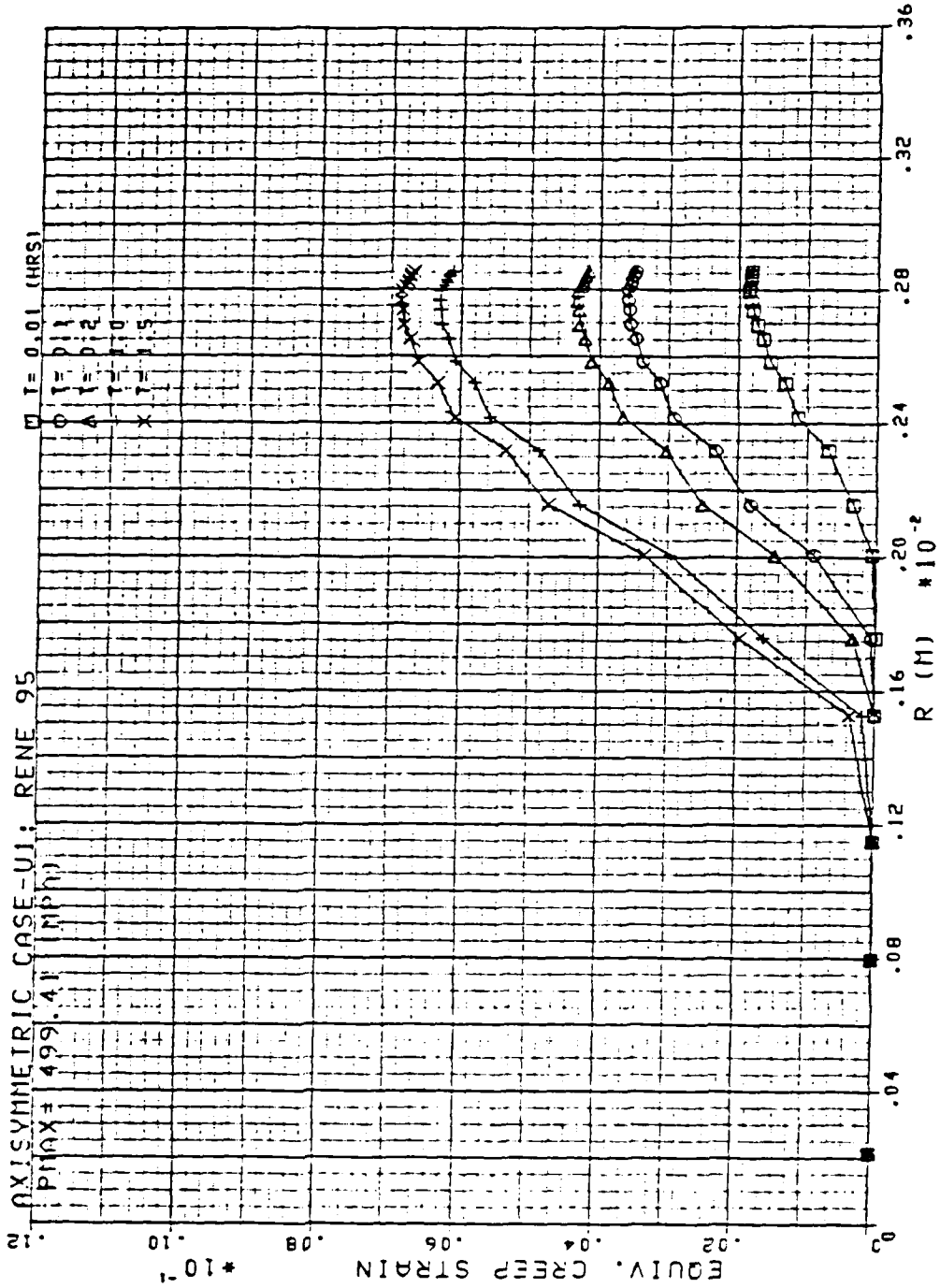

Figure 11 Equivalent Creep Strain Profile Along Minimum Cross-Section of U-Notched Specimen

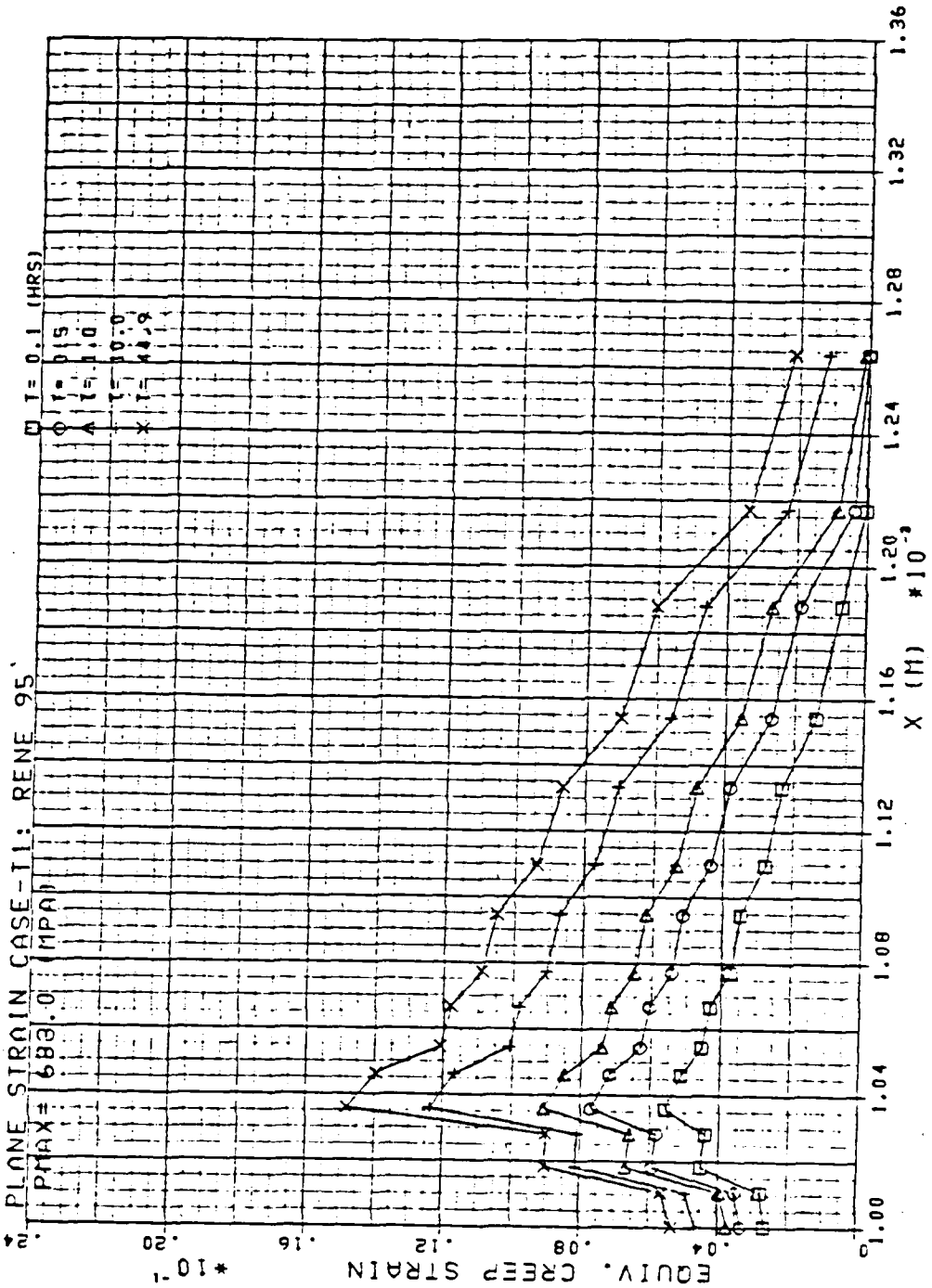

Figure 12 Equivalent Creep Strain Distribution Along Minimum Cross-Section Close to Notch Tip of a Type 4 Notch Specimen

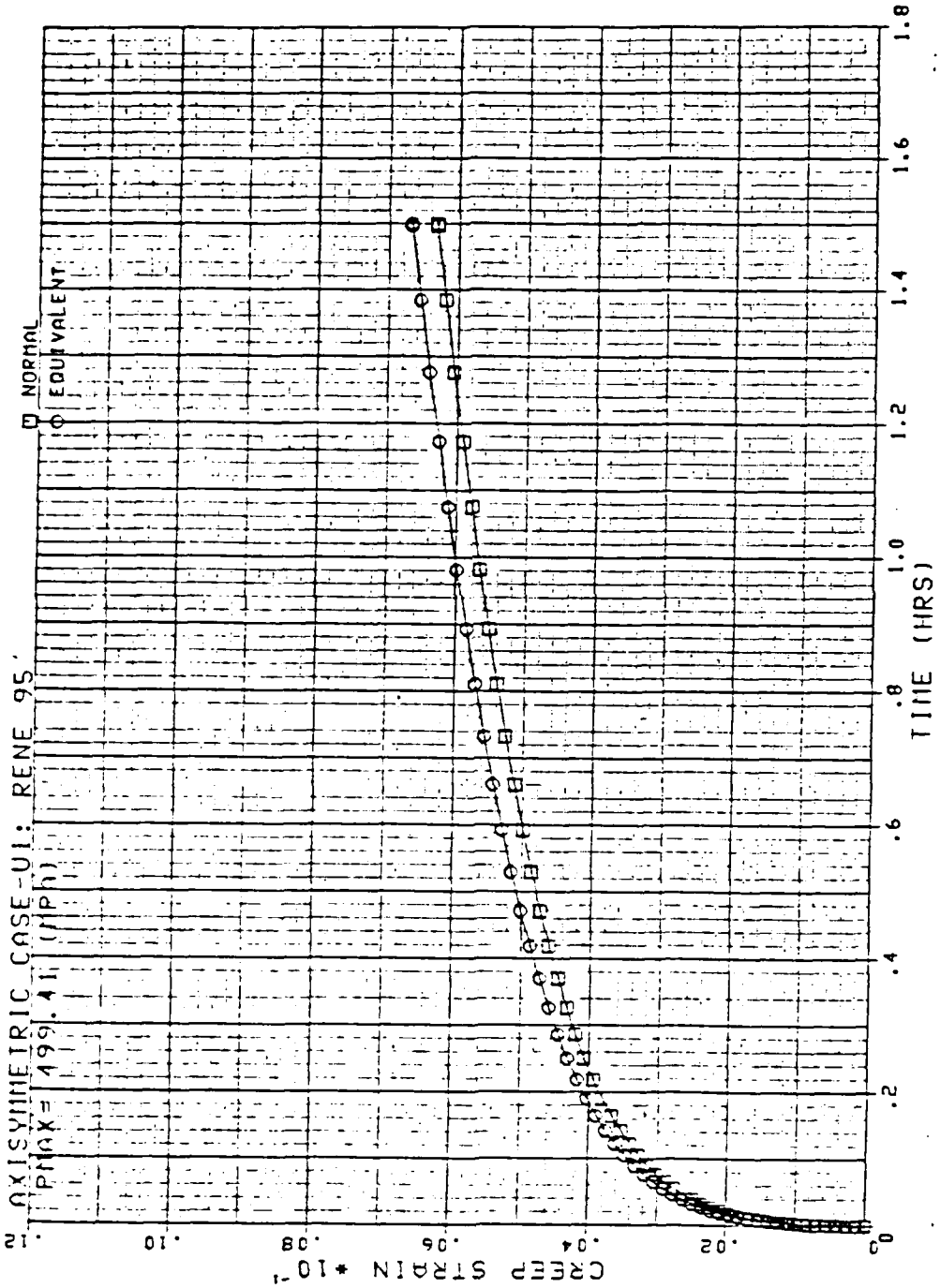

Figure 13 Creep Strain History at Notch Tip of a U-Notched Specimen

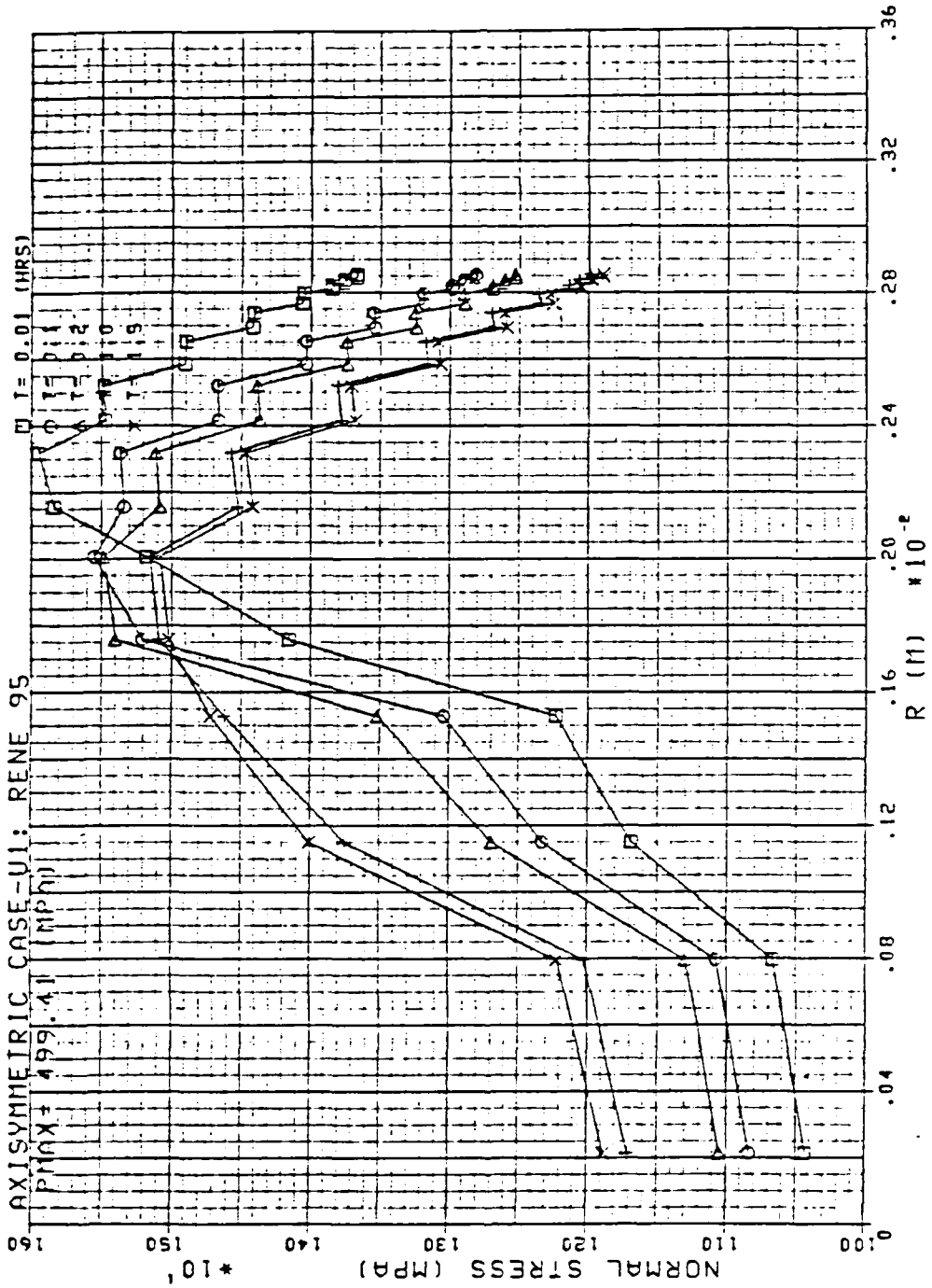

Figure 14 Normal Stress Profile Along Minimum Cross-Section of a U-Notched Specimen

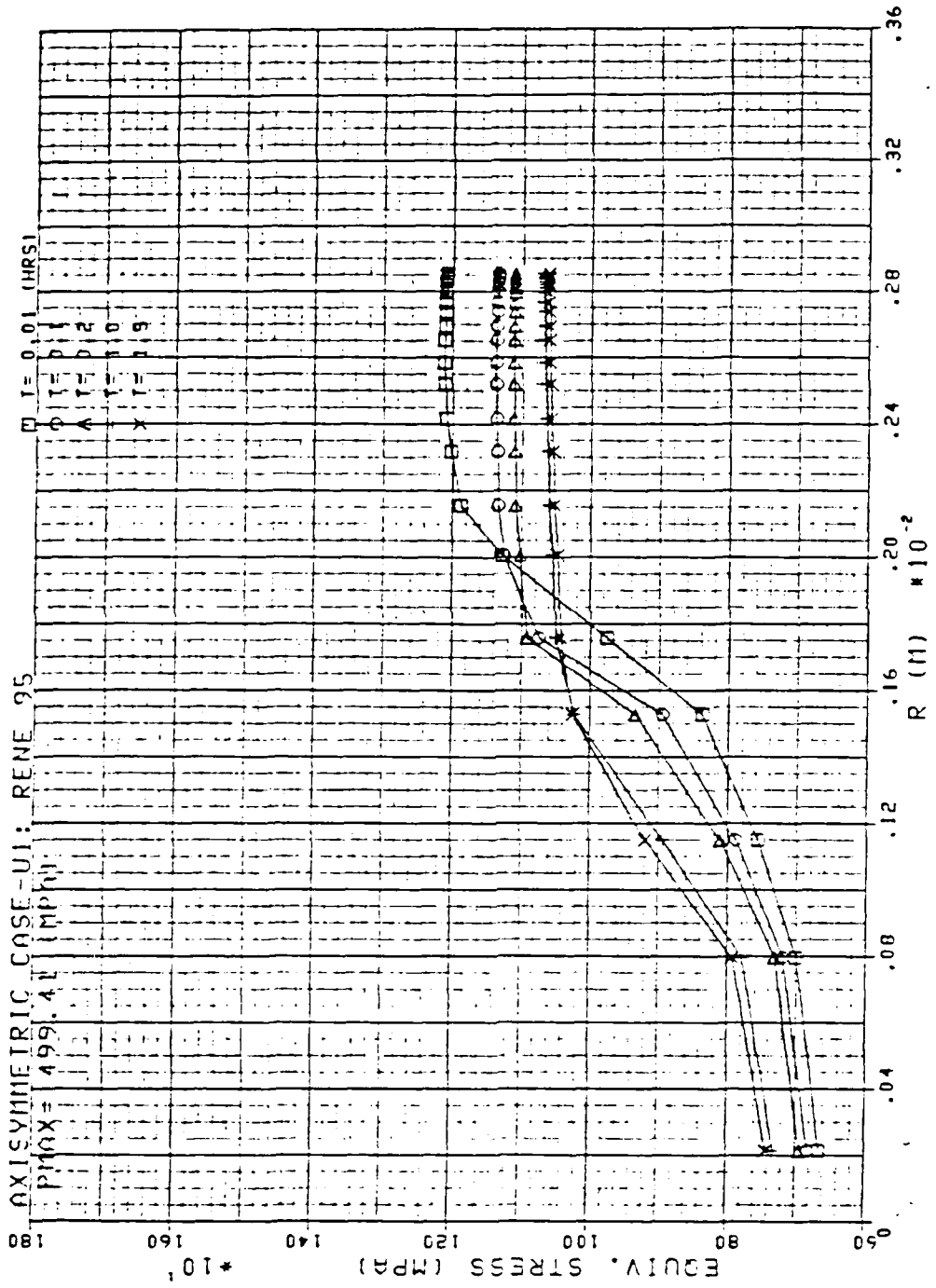

Figure 15 Equivalent Stress Profile Along Minimum Cross-Section of a U-Notched Specimen

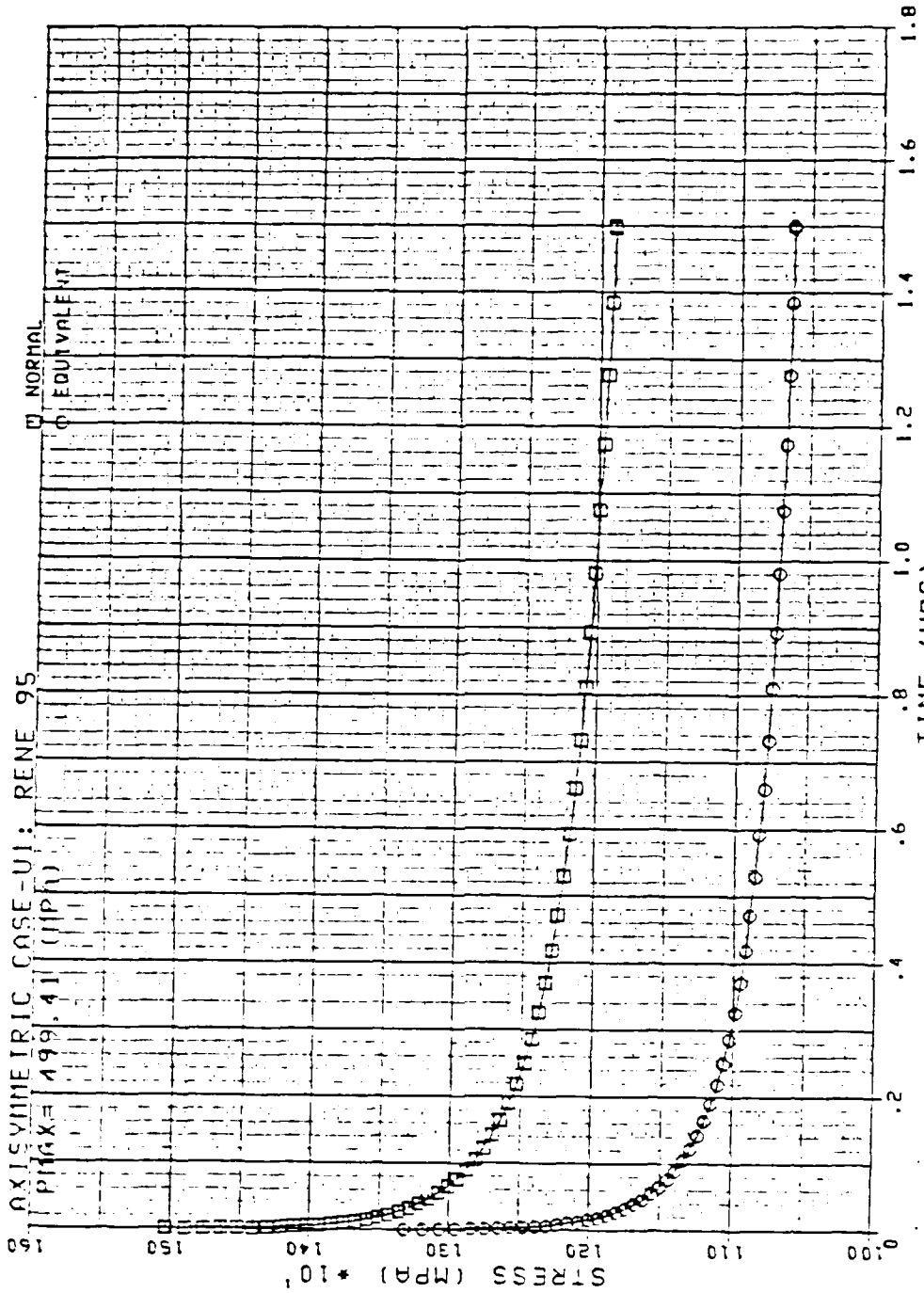

Figure 16 Time History of Stresses at the Notch Tip of a U-Notched Specimen

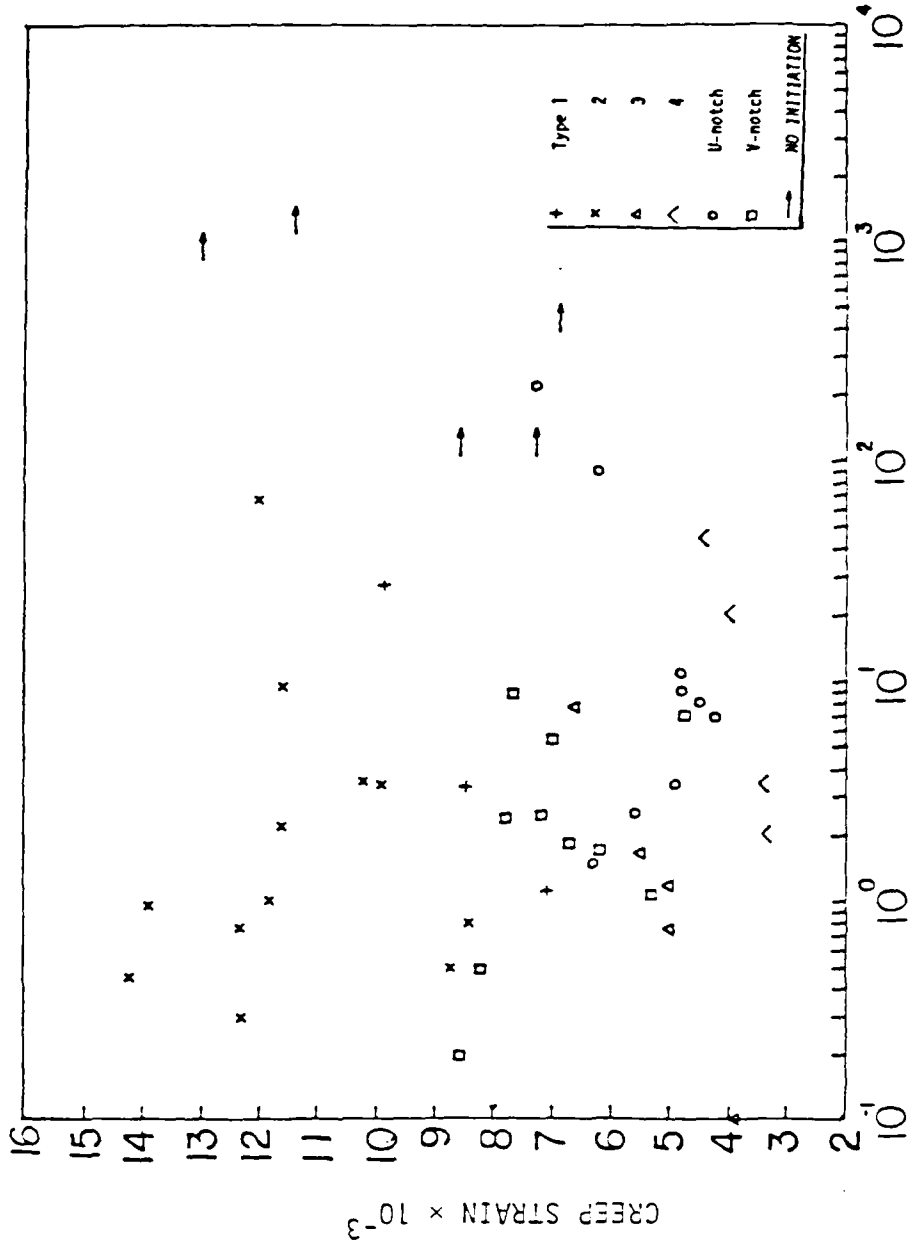

Figure 17 Normal Creep Strain at the Notch Tip vs. Initiation Time

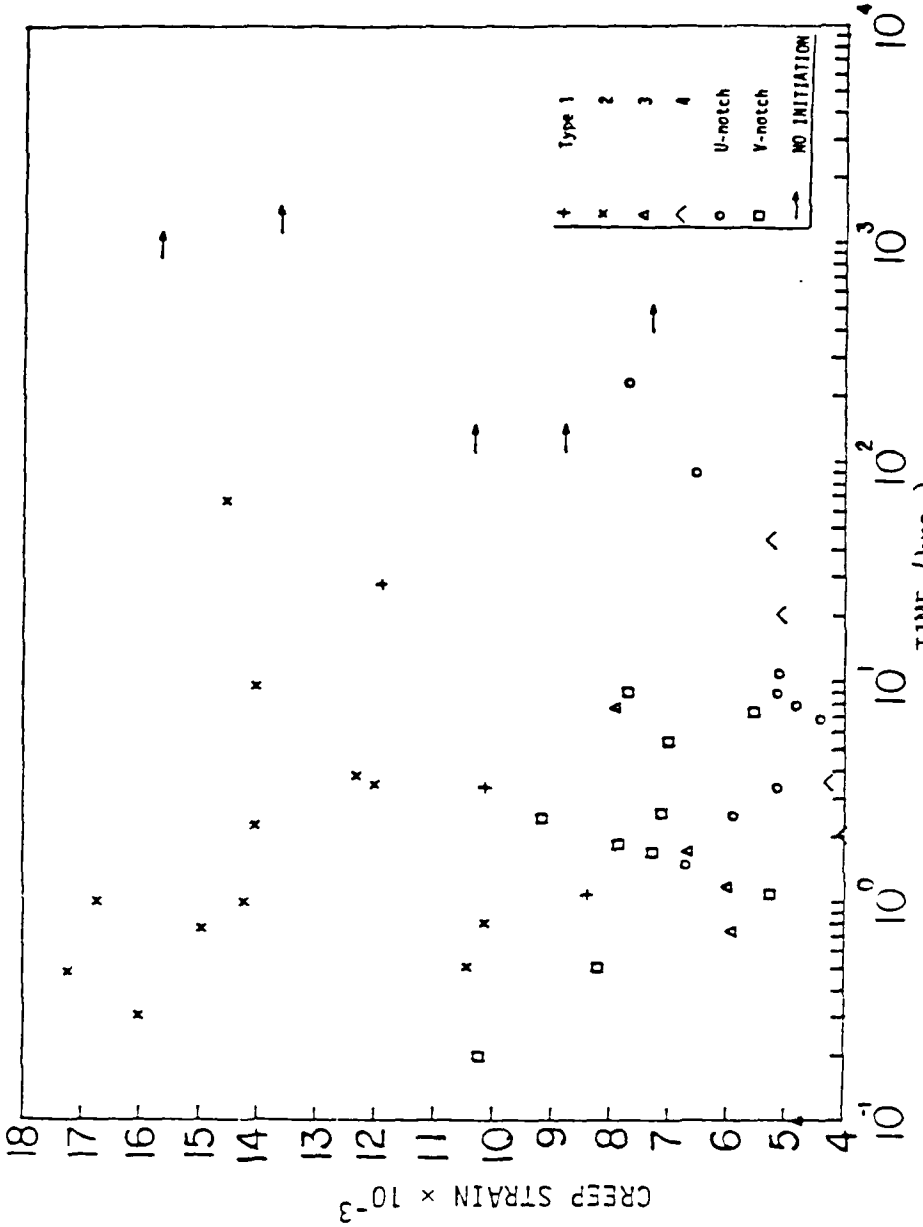

Figure 18 Equivalent Creep Strain of the Notch Tip vs. Initiation Time

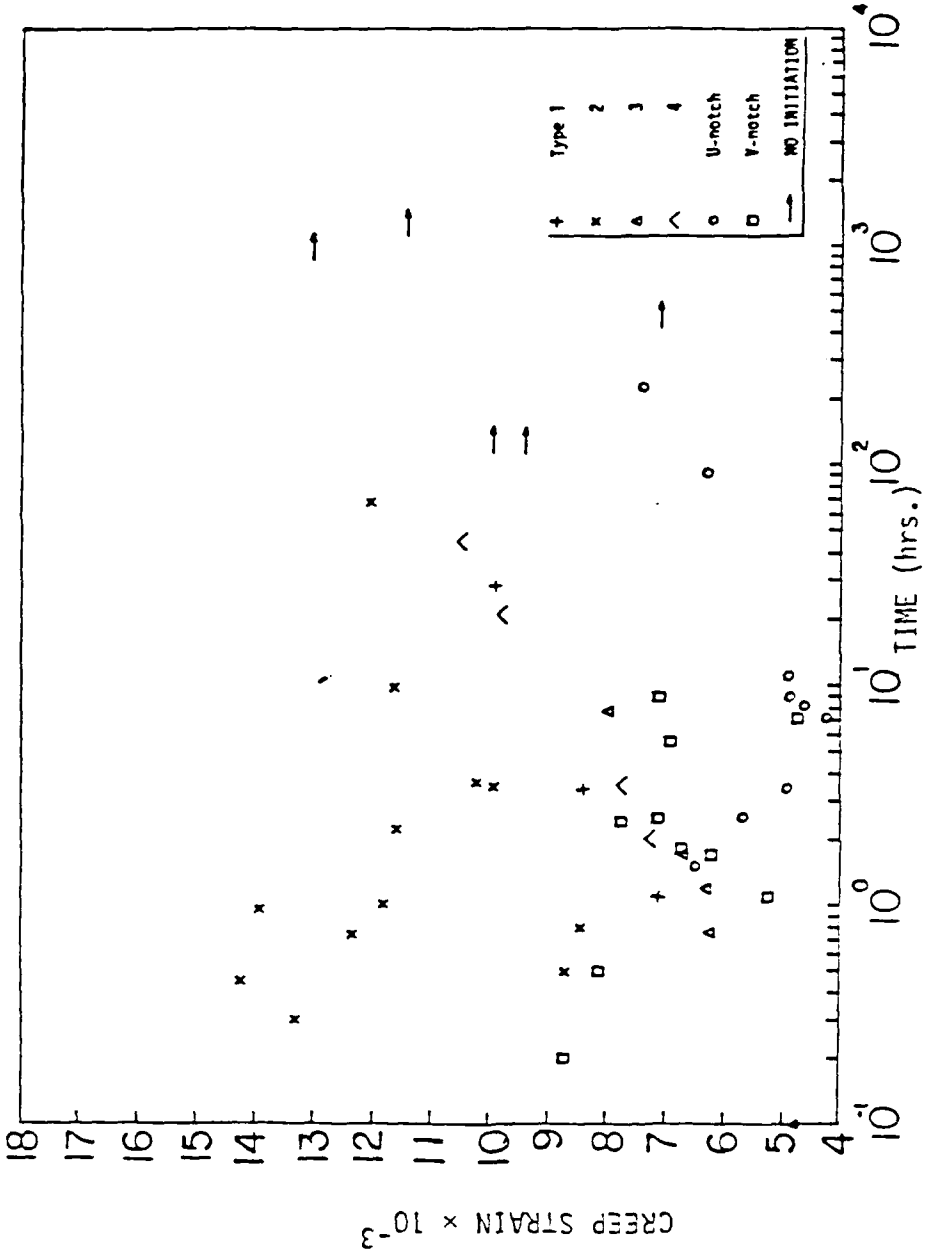

Figure 19 Maximum Normal Creep Strain at Minimum Cross-Section vs. Initiation Time

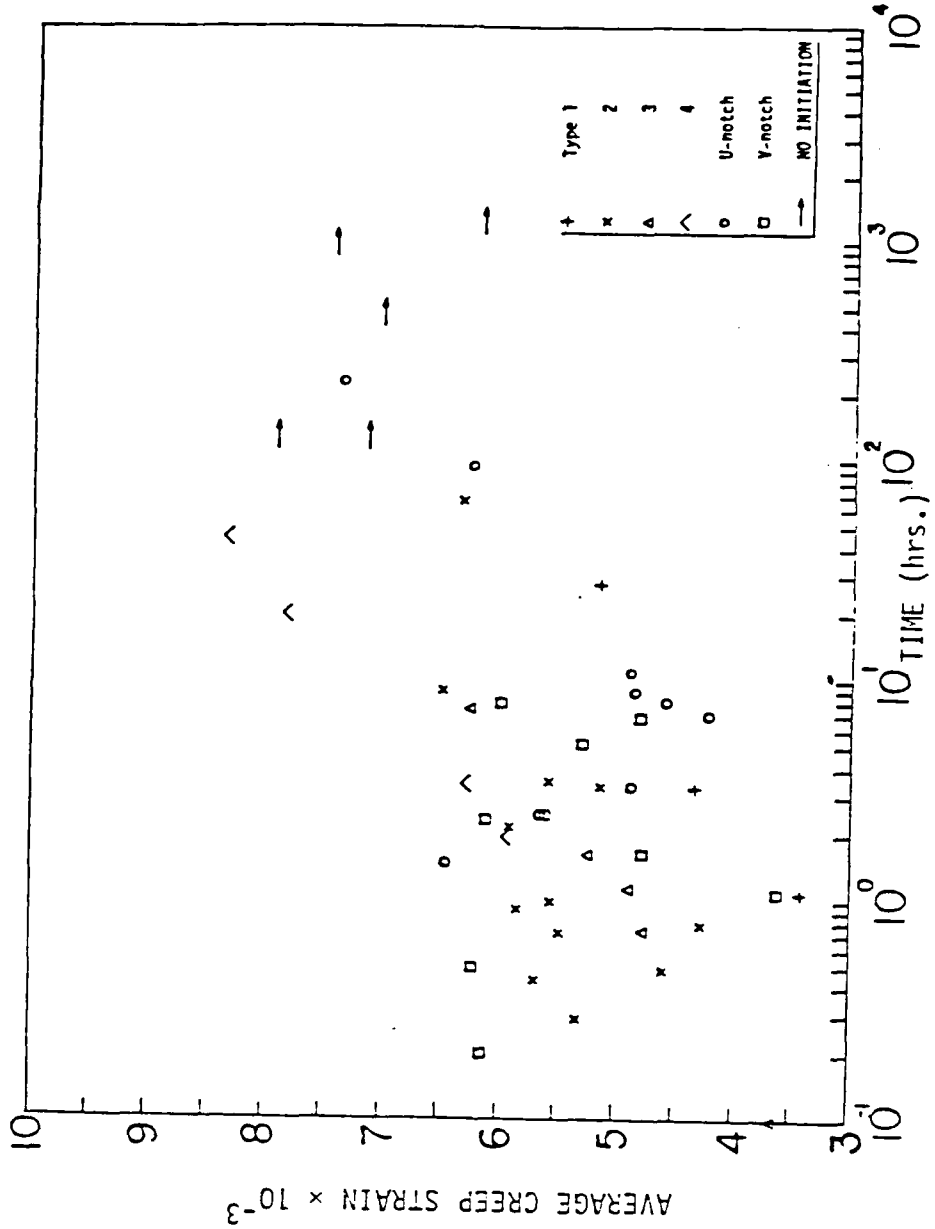

Figure 20 Average Normal Creep Strain over 100 Microns vs. Initiation Time

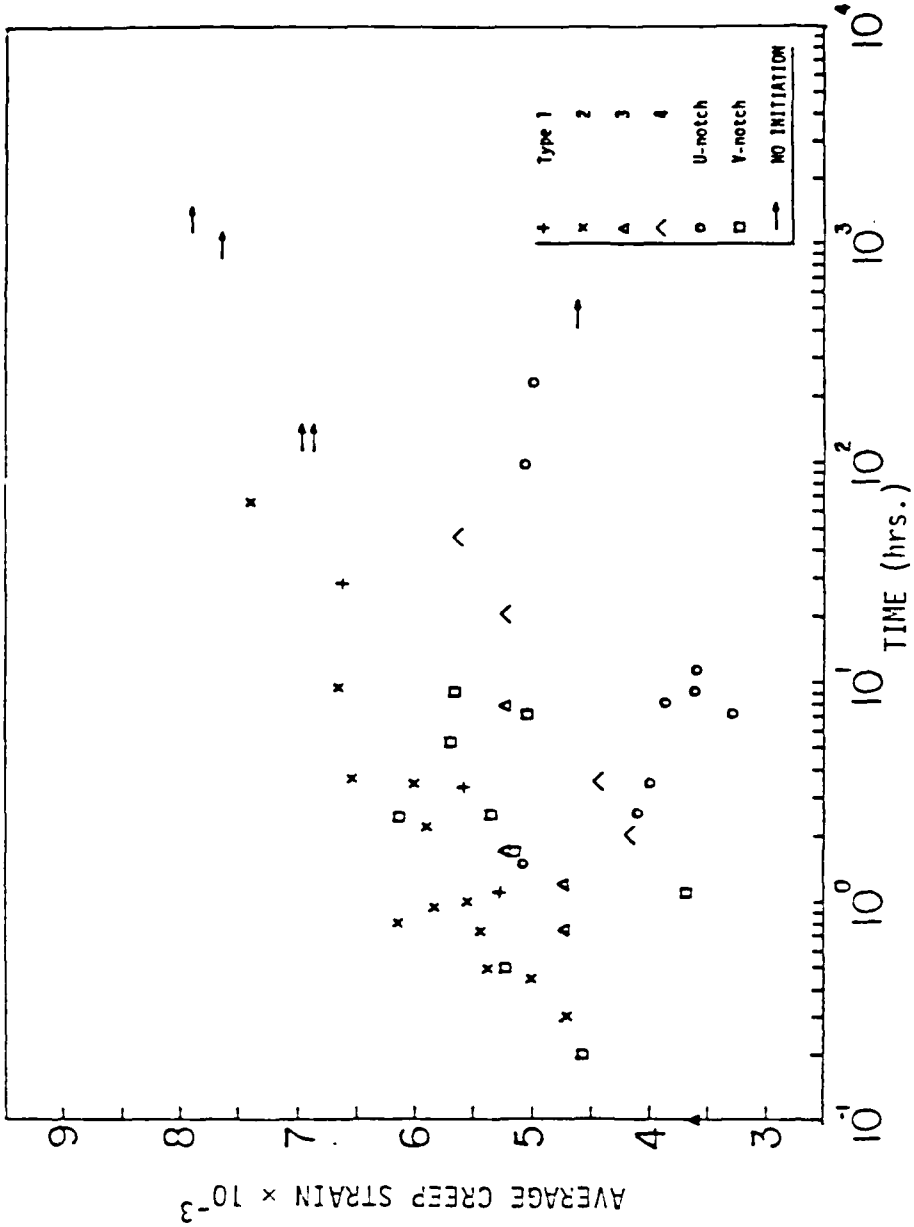

Figure 21 Average Normal Creep Strain over CDPZ vs. Initiation Time

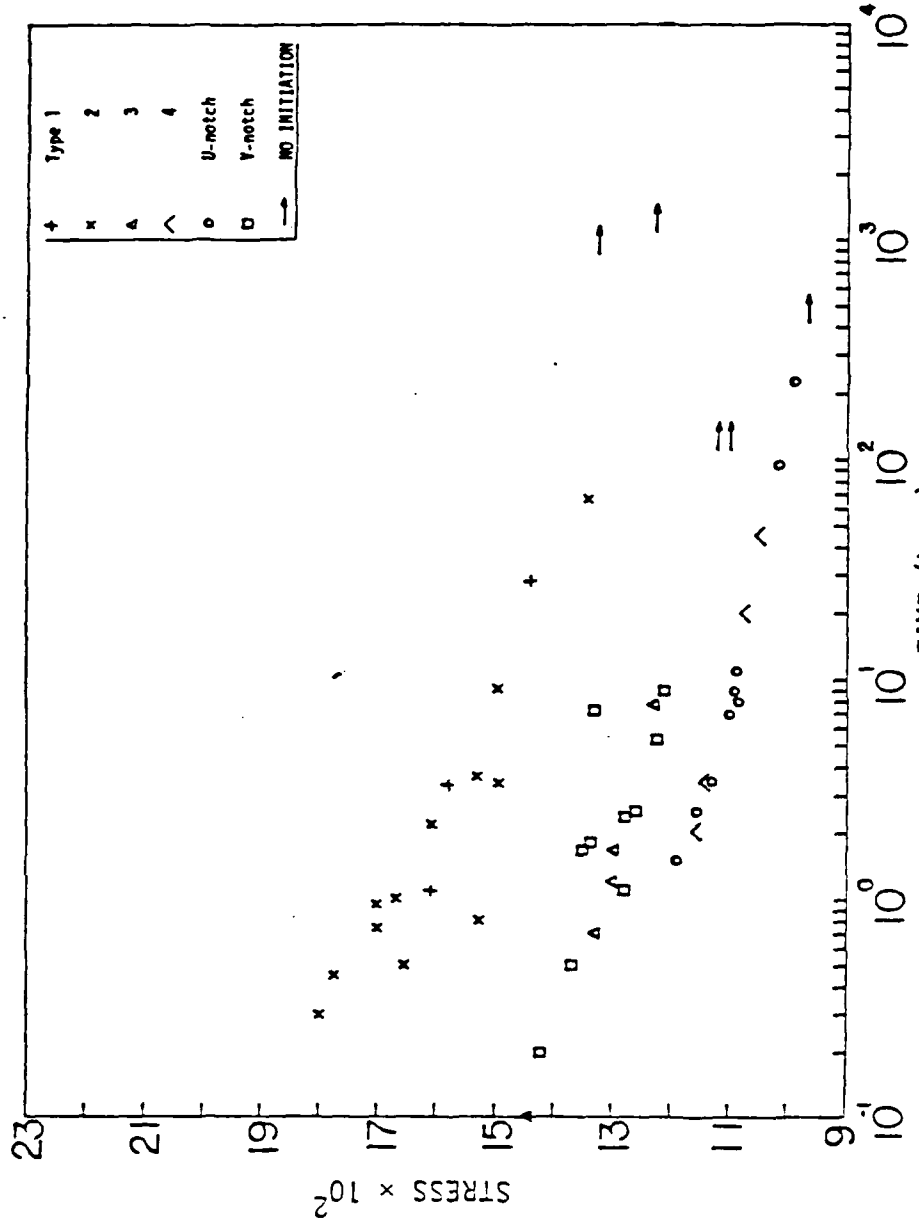

Figure 22 Normal Stress at Notch Tip at Initiation vs. Initiation Time

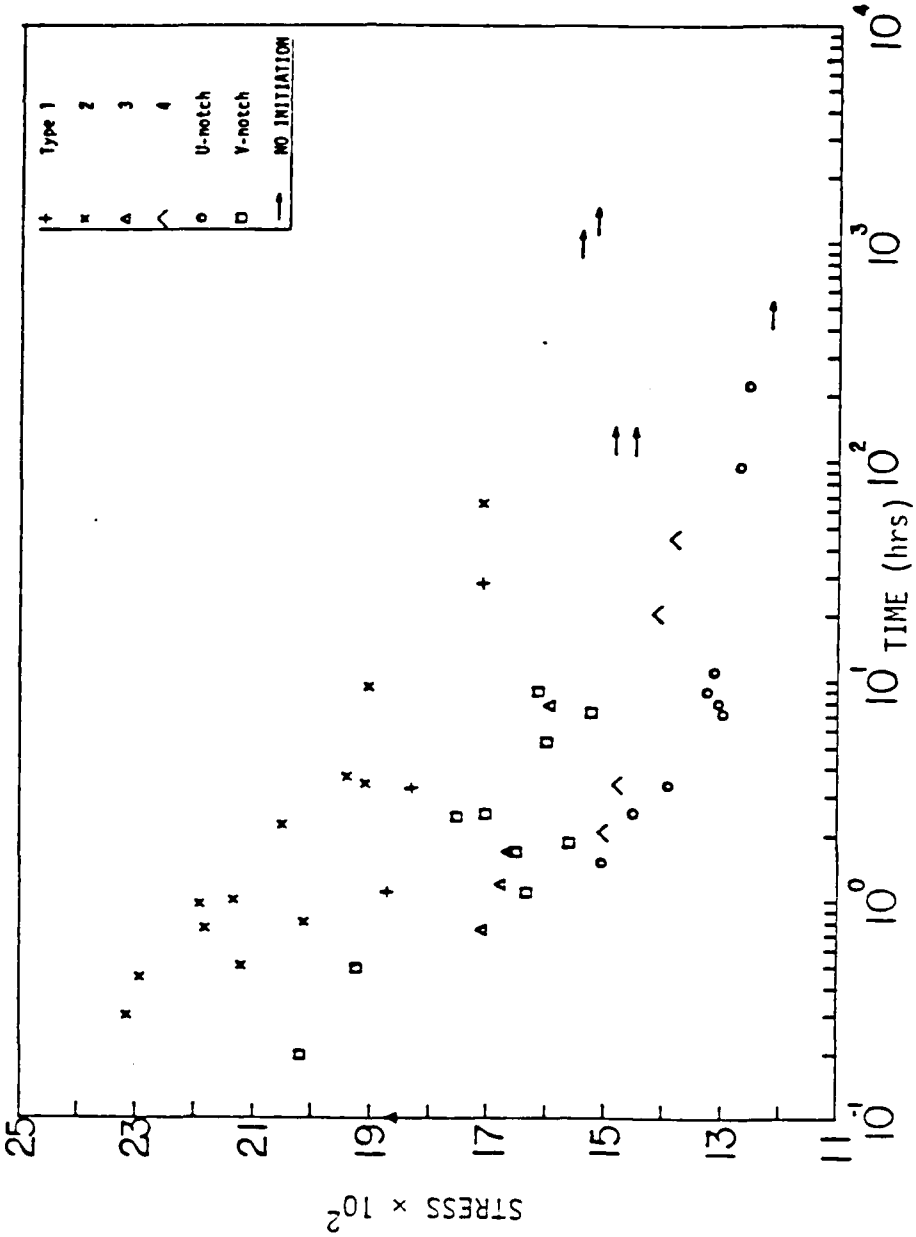

Figure 23 Maximum Normal Stress at Minimum Cross-Section at Initiation vs. Initiation Time

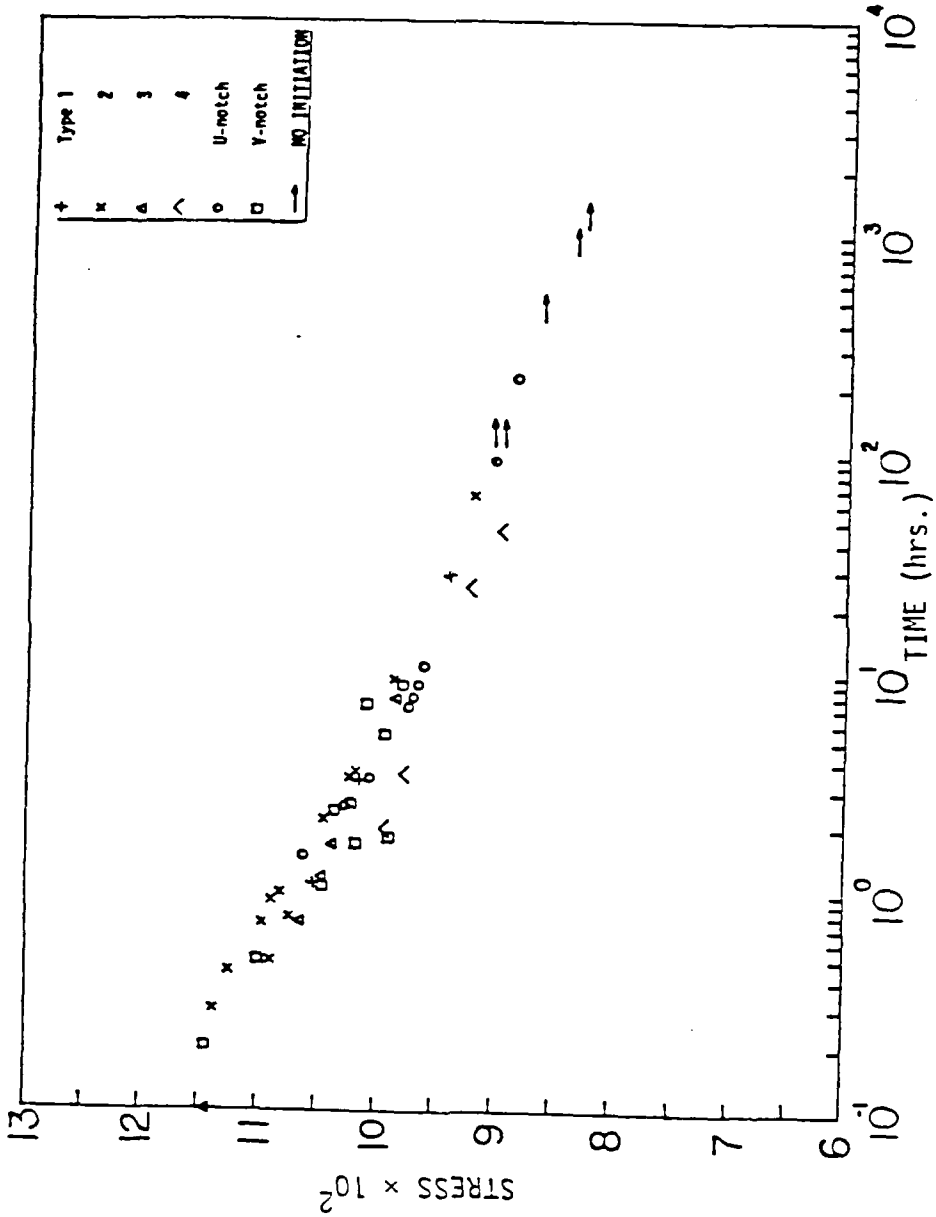

Figure 24 Equivalent Stress at Notch Tip at Initiation vs. Initiation Time

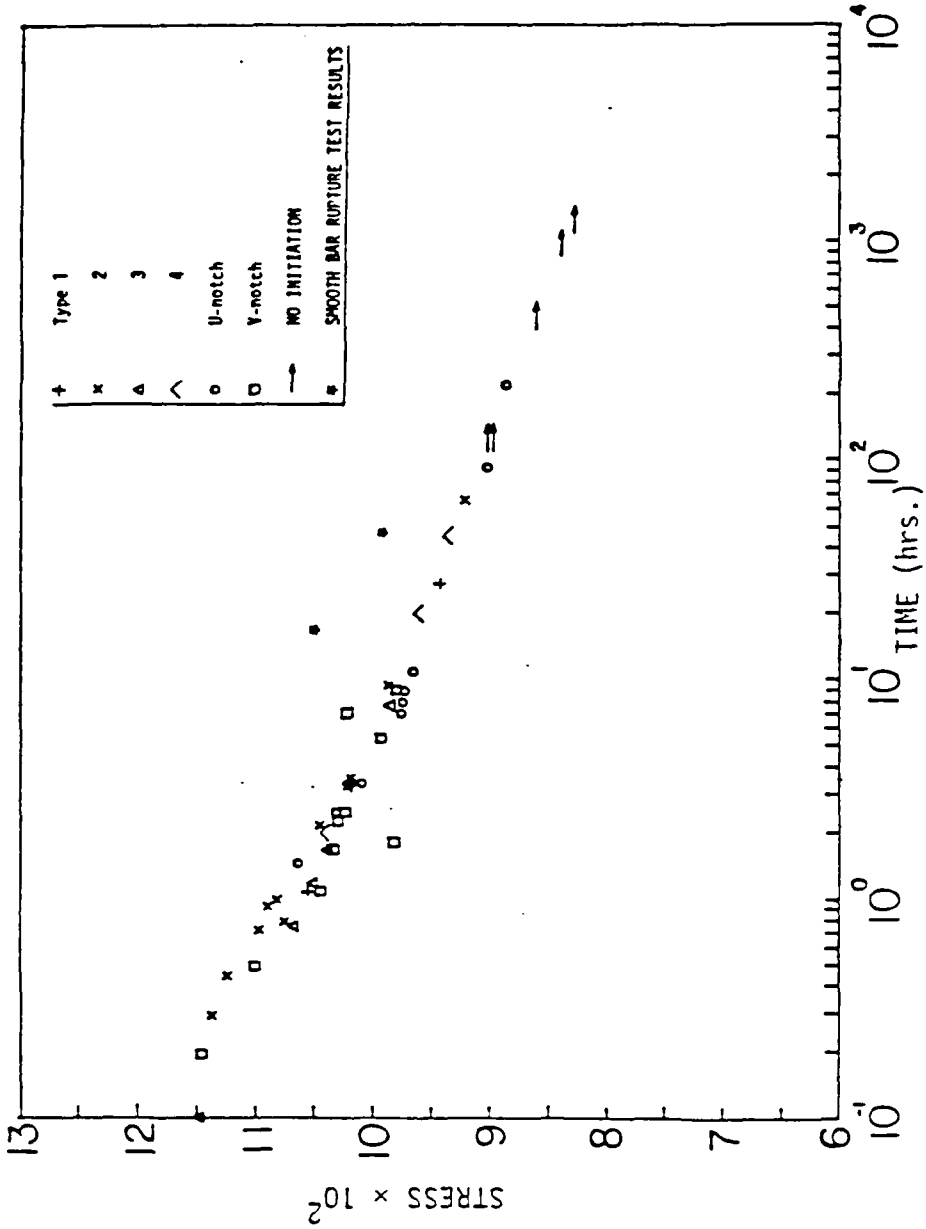

Figure 25 Maximum Equivalent Stress at Minimum Cross-Section at Initiation vs. Initiation Time

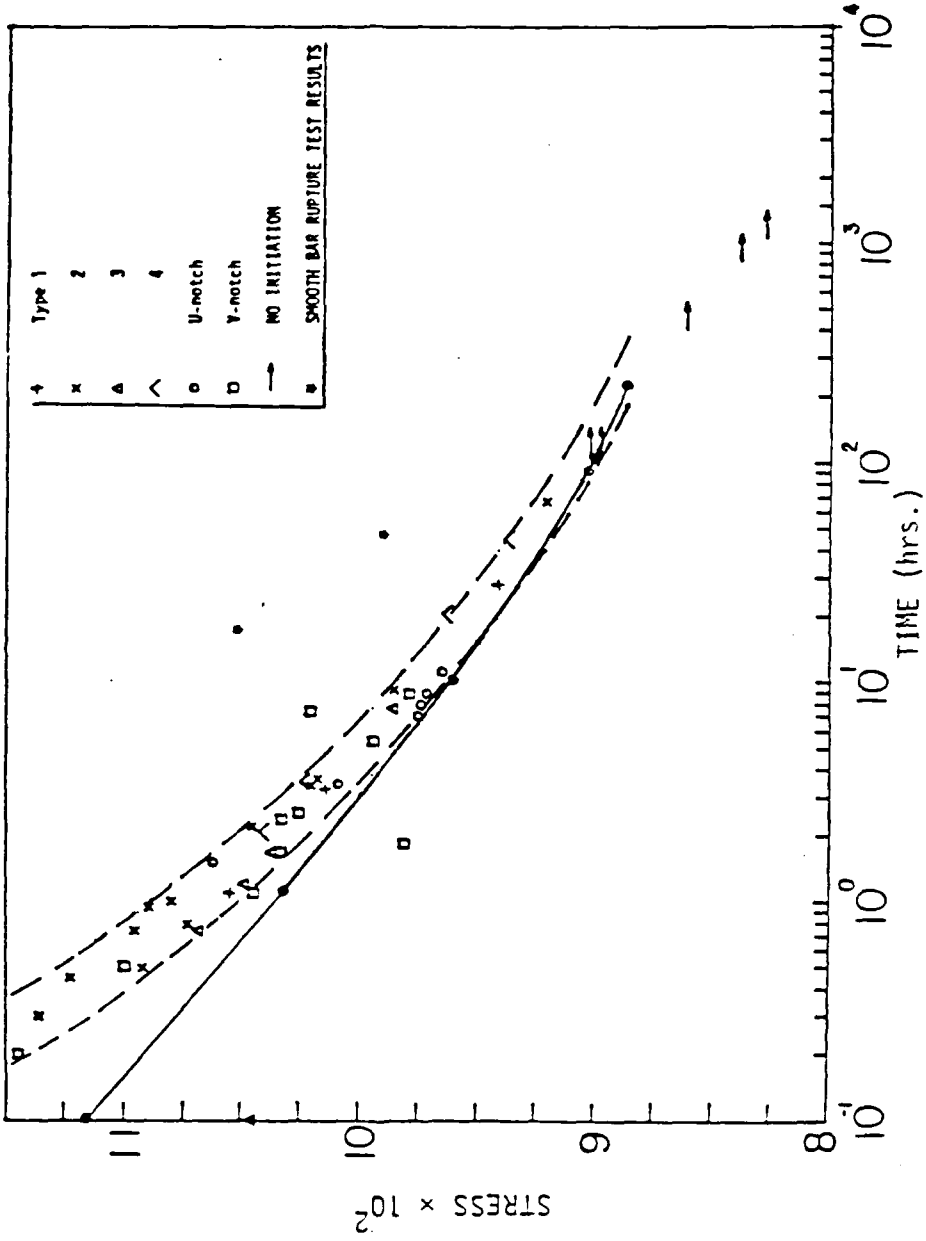

Figure 26 Time History of Maximum Equivalent Stress at Minimum Cross-Section at Initiation for Test #7 of U-Notched Specimen. (σ^{∞} = 414.51 MPa, t_i = 224.9 hrs.)

END

DTIC

9-86